

# **Simulating Fluid-Structure Interaction in Smoothed Particle Hydrodynamics Method**

by

©Xiangda Cui

A Thesis submitted to the School of Graduate Studies in partial fulfillment of the  
requirements for the degree of

**Master of Engineering**

**Faculty of Engineering and Applied Science**

Memorial University of Newfoundland

**May 2018**

St. John's

Newfoundland

# Abstract

In this thesis, a numerical program based on an improved smoothed particle hydrodynamics (SPH) method has been developed to solve the nonlinear fluid-structure interaction problems. The program simulates breaking free-surface flows and evaluates the global and local hydrodynamic loads on structures.

In the present SPH method, the fluid domain is discretized into fluid particles which allows the Euler equation to be numerically solved. A kernel function is employed to interpolate the flow field and the approximate Euler equations explicitly. The solid boundaries are modelled using a fixed ghost particle method. A diffusive term was adopted to smooth the noise in the pressure field. A particle shift technique was adopted and improved by introducing a layer of background particles along the free surface to minimize the interpolation error caused by the anisotropic particle distribution.

Validation studies were carried out in three two-dimensional cases including dam-break flow impacting against a vertical wall, water entry of a free-fall wedge, and sloshing flow in a rectangular container excited by roll motions. The numerical results were compared with the experimental results and other published numerical solutions.

# Acknowledgements

I would like to express my gratitude to my supervisor, Dr. Qiu, for his continuous support, encouragement and fruitful ideas throughout my research. With his patient guidance, I have experienced a fruitful research project in which I not only got a comprehensive understanding about marine hydrodynamics but also a professional attitude to my academic career.

I am grateful to the financial support by the NSERC CREATE Training Program.

I would like to give thanks to my colleagues in Advanced Marine Hydrodynamics Laboratory at Memorial University. I really appreciate their friendship and encouragements.

Finally, I want to express appreciation to my parents, brother, sister-in-law and nephews for their endless love and support.

# Table of Contents

<b>Abstract</b>	<b>i</b>
<b>Acknowledgments</b>	<b>ii</b>
<b>Table of Contents</b>	<b>v</b>
<b>List of Figures</b>	<b>viii</b>
<b>Nomenclature</b>	<b>viii</b>
<b>1 Introduction</b>	<b>1</b>
1.1 Background and Motivation . . . . .	1
1.2 Literature Review . . . . .	2
1.2.1 Smoothed particle hydrodynamics . . . . .	2
1.2.2 SPH in the free-surface flows . . . . .	3
1.2.2.1 Slamming . . . . .	3
1.2.2.2 Sloshing . . . . .	5
1.2.2.3 Water waves . . . . .	6
1.2.2.4 Wave-body interactions . . . . .	7
1.2.3 Major drawbacks and improvements in the SPH method . . . . .	9
1.2.3.1 Boundary conditions . . . . .	9

1.2.3.2	High frequency noise in pressure field . . . . .	10
1.2.3.3	Viscosity and numerical instability . . . . .	12
1.3	Overview . . . . .	13
<b>2</b>	<b>Mathematical Formulation</b>	<b>14</b>
2.1	Governing Equations . . . . .	14
2.1.1	Equations of Momentum . . . . .	14
2.1.2	Continuity Equation and Equation of State . . . . .	15
2.2	SPH Method . . . . .	16
2.2.1	Integral Interpolation . . . . .	16
2.2.2	Integral Interpolation of Differential Operators . . . . .	19
2.2.3	Standard SPH Equations . . . . .	21
2.2.4	SPH Equations with numerical diffusive and viscous terms . . . . .	22
2.3	Boundary Conditions . . . . .	23
2.3.1	Free-surface Boundary Condition . . . . .	23
2.3.2	Solid Boundary Condition . . . . .	24
2.4	Particle shift technique . . . . .	27
2.4.1	Disordered particles distribution problem . . . . .	27
2.4.2	Particle shift formulations . . . . .	29
2.4.3	Background particles along the free surface . . . . .	30
2.5	Numerical Implementations . . . . .	34
2.5.1	Gaussian Kernel . . . . .	34
2.5.2	Choice of time schemes . . . . .	34
2.5.3	Global Forces on Floating Bodies . . . . .	35
2.5.4	Equations of motion for a floating body . . . . .	37
2.6	Summary of the computation . . . . .	37

<b>3 Numerical Results</b>	<b>40</b>
3.1 Dam-break flow . . . . .	40
3.1.1 Case description . . . . .	40
3.1.2 Convergence study . . . . .	41
3.1.3 Simulation results . . . . .	43
3.2 Water entry . . . . .	50
3.2.1 Case description . . . . .	50
3.2.2 Convergence study . . . . .	52
3.2.3 Simulation results . . . . .	53
3.3 Sloshing flow . . . . .	60
3.3.1 Case description . . . . .	60
3.3.2 Convergence study . . . . .	62
3.3.3 Numerical results . . . . .	63
<b>4 Conclusions and Future Work</b>	<b>67</b>
<b>Bibliography</b>	<b>69</b>

# List of Figures

2.1	Smoothing kernel . . . . .	17
2.2	Gaussian kernel function . . . . .	18
2.3	Incomplete kernels truncated by boundary surfaces . . . . .	20
2.4	Sketch of an incomplete kernel supplemented by fixed ghost particles	25
2.5	Interpolation points of fixed ghost particles . . . . .	25
2.6	Sketch of the interpolation of the fixed ghost particle . . . . .	26
2.7	Sketch of the velocity of the fixed ghost particle . . . . .	27
2.8	Anisotropic particle distribution in dam-break flow . . . . .	28
2.9	Distribution of initial background particles . . . . .	32
2.10	Active background particles . . . . .	32
2.11	Neighbour particles of background particles . . . . .	33
2.12	Background particles and fluid particles . . . . .	33
2.13	Flowchart of the numerical algorithm . . . . .	39
3.1	Sketch of the setup of the dam-break test . . . . .	41
3.2	Sensitivity of the pressure on $P_1$ to the particle spaces . . . . .	42
3.3	Sensitivity of the pressure on $P_1$ to the time step sizes . . . . .	42
3.4	Comparison between the flow fronts measured by the simulation and experiments . . . . .	44

3.5	Comparison between the flow heights measured by the simulation and experiments at probe $H_1$ . . . . .	44
3.6	Comparison between the pressures measured at probe $P_1$ with $ds=0.002m$	45
3.7	Comparison between the pressures measured at probe $P_2$ with $ds=0.002m$	45
3.8	Particle distribution near pressure sensor $P_1$ in dam-break flow by the original SPH method (top) and the present SPH method (below) . . .	46
3.9	Snapshots of the evolution of the dam-break flow at $t(g/H)^{1/2} = 1.58$	47
3.10	Snapshots of the evolution of the dam-break flow at $t(g/H)^{1/2} = 3.27$	48
3.11	Snapshots of the evolution of the dam-break flow at $t(g/H)^{1/2} = 5.85$	49
3.12	Sketch of the water entry of a wedge . . . . .	50
3.13	Distribution of the fluid particles and solid ghost particles . . . . .	51
3.14	Sensitivity of the slamming force to particle spacing . . . . .	52
3.15	Sensitivity of the slamming force to time step size . . . . .	53
3.16	Time history of the velocity of the wedge during the drop test . . . .	55
3.17	Time history of the slamming force on the wedge during the test . . .	55
3.18	Particle distribution profiles predicted by the original SPH method (top) and the present SPH method (below) . . . . .	56
3.19	Pressure distribution on the wedge at $t=0.00435s$ and $ds=B/300$ . . .	57
3.20	Pressure distribution on the wedge $t=0.0158s$ and $ds=B/300$ . . . . .	58
3.21	Pressure distribution on the wedge at $t=0.0202s$ and $ds=B/300$ . . .	59
3.22	Sketch of the setup of the sloshing tank . . . . .	60
3.23	Time history of the angular velocity of the tank by Delorme et al. (2009)	61
3.24	Time history of the angle of the tank by Delorme et al. (2009) . . . .	61
3.25	Sensitivity of the impact pressure on $P_1$ to particle spacing . . . . .	62
3.26	Sensitivity of the impact pressure on $P_1$ to time step size . . . . .	63
3.27	Time history of impact pressure on $P_1$ . . . . .	64

3.28	Snapshots of the evolution of the sloshing flow at $t=2.40s$ . . . . .	65
3.29	Snapshots of the evolution of the sloshing flow at $t=3.40s$ . . . . .	66

# Nomenclature

$\mathbf{u}$	Velocity
$\rho$	Density
$p$	Pressure
$\mathbf{r}$	Position
$V$	Volume
$m$	Mass
$c$	Speed of sound
$\mathbf{g}$	Gravity
$W$	Smoothing function or kernel
$h$	Smoothing length
$\alpha$	Artificial viscosity coefficient
$\delta$	Diffusive coefficient in continuity equation
$\mathbf{n}$	Unit normal vector
$\boldsymbol{\tau}$	Unit tangent vector
$i$	The particle of interest
$j$	Neighbour particles
$\nabla p$	Gradient of pressure
$\nabla \cdot \mathbf{u}$	Convergence of velocity

# Chapter 1

## Introduction

### 1.1 Background and Motivation

Offshore structures under extreme sea conditions can experience several types of impact flows such as slamming, sloshing, and green water on deck (Mei (1989)). The evaluation of the global and local hydrodynamic loads caused by these violent fluid-structure interactions is important for the design of offshore structures. Since these non-linear problems are usually coupled with strong dynamics, largely deformed or breaking free surface and fluid segments, their analysis can be very complex. Analytical methods are only applicable to simple cases, while experiments are expensive and time-consuming. In this context, the computational fluid dynamics (CFD) methods based on solving the Navier-Stokes equations become very popular and useful because they can solve these complex fluid problems with relatively lower cost. Moreover, the CFD methods can also provide valuable information that can reveal the physical mechanism behind the flow phenomena.

## 1.2 Literature Review

### 1.2.1 Smoothed particle hydrodynamics

In computational fluid dynamics, there are two main ways to solve governing equations. One is the Lagrangian approach in which the individual fluid particle is tracked, and its physical quantities are recorded. The other is the Eulerian approach in which the physical fields are investigated on fixed space.

Based on the Eulerian approach, the finite volume method (FVM) and the finite difference method (FDM) have been widely applied to computational fluid dynamics for decades (Chung (2010)). CFD methods can solve these complex fluid problems with relatively lower cost compared with experiments. However, CFD simulations can be faced with challenges when the flow is accompanied by moving boundaries or complex interfaces. Surface tracking or capturing methods are employed to handle these interfaces. Surface tracking methods have to keep updating the meshes as the flow evolves. When the interface is largely deformed, the re-meshing procedure can be too difficult to perform. The surface capturing methods are more flexible because they do not require mesh updates, but they give less accurate presentation of the interface (Tezduyar (2002)). As a fully Lagrangian CFD method, the smoothed particle hydrodynamics (SPH) method can easily model interfaces. This method has been successfully applied to various fluid flows.

It is an intuitive idea to employ particles to model the fluid flows, considering the fact that the fluid flows are composed of molecules in nature. The SPH method was first proposed independently by Gingold and Monaghan (1977) and Lucy (1977) to solve astrophysical problems. Compared with the mesh-based methods, using arbitrarily moving particles to interpolate the fluid flows is not easy. Gingold and Monaghan (1977) proposed an integral interpolation over the neighbour particles to

obtain the spatial derivatives of field functions. This interpolation method originating from the statistical theories and the Monte Carlo integrations is the basis of the SPH method (Marrone (2012)). In the following decade, this method was mainly applied to astrophysical problems. After the first application to the free-surface flows by Monaghan (1994), it was surprising to find that this method could be applied to various fluid, solid elastic and solid fracture problems, benefiting from their Lagrangian character (Monaghan (2005)). The following literature review is mainly focused on the development of the SPH method in free-surface flows.

## **1.2.2 SPH in the free-surface flows**

The SPH method has been widely applied to free-surface flows. Monaghan (1994) first developed the SPH method to simulate free-surface flows, with a repellent force particle technique to model solid boundaries. In this paper, it was assumed that the fluid was weakly compressible while a specialized equation of state was designed to relate the density field and pressure field explicitly. Reasonable evolution of the free-surface flows was obtained without special treatments to enforce the free-surface conditions. This paper developed the basic framework of the SPH method, and it is also the origin of the numerous applications in fluid flows. Following the work of Monaghan (1994), various problems in free-surface flows were investigated using the SPH method.

### **1.2.2.1 Slamming**

A structure entering the water is a key problem in marine hydrodynamics, and it is also an important application of the SPH method. Oger et al. (2004) first applied the SPH method to simulate the water entry of a wedge. In this work, the SPH results were compared with the numerical results of the FVM, proving the feasibility

of the SPH method in slamming. Although reasonable slamming forces were obtained, the water jet and splashing were not simulated properly because of the low particle resolutions.

Oger et al. (2005) studied the air cushion effect in water entry problem using a two-phase SPH model. In this article, both the air and water pressure were evaluated and coupled with the falling wedge. It was found that the two-phase SPH model could capture the air cushion effect, however, only gave less ideal results compared with the experimental ones. Oger et al. (2006) further studied water entry problem using a variable smoothing length technique to realize the spatially varying resolution in the SPH method. Benefiting from this technique, an extremely high resolution was realized in the zone near the wedge, and the pressure distributions on the wedge surface were accurately evaluated.

Shao (2009) used an incompressible SPH method to simulate the free surface deformations and evaluate the global impact loads. This method used less particles than the SPH method, but smoother numerical results were obtained. The aforementioned works were limited within two-dimensional simulations.

Maruzewski et al. (2010) developed a three-dimensional parallelized SPH model to study various rigid bodies impacting on the free surface. In this work, a maximum of one hundred million particles were employed to model the water entry of a solid ball. In another case of a full ship hull impacting on the free surface, only two million particles were employed to evaluate the slamming force costing 24 hours on 16 cores. Reasonable slamming force series were obtained comparing with the experimental ones. This application proved that the SPH method could solve the engineering problems with an affordable computational cost.

Veen and Gourlay (2011) used a two-dimensional SPH method to model water entry of various sections, including wedge, flared hull section and catamaran hull

section to evaluate the slamming loads and the falling velocities. Veen and Gourlay (2012) further combined this two-dimensional SPH algorithm with the strip theory to evaluate the slamming loads on a V-form ship hull. This work proved the ability of the SPH method to calculate slamming pressures for various two-dimensional hull section shapes. However, only poor agreement was obtained comparing the slamming force and motions predicted by the combined method with the results of experiments.

### 1.2.2.2 Sloshing

Souto-Iglesias et al. (2003) first applied the original SPH model by Monaghan (1994) to simulate sloshing flows in anti-roll tanks with obstacles. The largely deformed free surface was properly simulated, and the moment phase lags were compared with the test results. This work proved the SPH method was feasible in the sloshing flows.

Landrini et al. (2003) used a two-phase SPH model to simulate the sloshing waves. The wave elevations evaluated in the simulations had a good agreement with the experimental results, while the sloshing forces and moments only reached an unsatisfying agreement. It was proved that this model had advantages to simulate the overturning of the free surface and the following fluid-fluid impact compared with the traditional methods.

Souto-Iglesias et al. (2006) accurately evaluated the sloshing moment amplitude using an improved repellent force solid boundary condition and a leap frog predictor-corrector time scheme.

Delorme et al. (2009) investigated the impact pressure in shallow water sloshing flows with both the experiments and SPH simulations. A density re-initialization procedure was adopted to smooth the pressure field, and reasonable pressure results were obtained. In order to accurately evaluate the impact pressure, some alternative approaches were applied to the sloshing problems.

Rafiee et al. (2012) adopted a Godunov-type SPH method, which was based on the solution of the local Riemann problem. This method gave an accurate and smooth prediction of the impact pressure, although it took a higher computational cost. Khayyer and Gotoh (2009) employed the incompressible SPH method to evaluate the sloshing impact loads. A high-order source term was used in the Poisson equation, and an improved detection method was employed to spot the fluid particles on the free surface. This work presented the advantages of the incompressible SPH method in the evaluation of the impact pressure in sloshing problems.

Gotoh et al. (2014) further enhanced the incompressible SPH method with a higher order Laplacian model and an error-compensating source. The time predictions of the impact pressures were compared with the experimental ones, and good agreement was reached. Although the incompressible SPH methods are more accurate in sloshing problems, the weakly compressible SPH method, which is more robust and time-saving, has been combined with the finite element method to deal with the coupled seakeeping-sloshing problems in Servan-Camas et al. (2016).

### 1.2.2.3 Water waves

In the early stage of its application, the SPH method was mainly applied to study near-shore water waves. Monaghan and Kos (1999) simulated solitary waves and their interactions with various dry beaches. Monaghan and Kos (2000) studied Scott Russell's wave generator with both experiments and SPH simulations, in which a falling box was used to generate a solitary wave in a rectangular tank. The experimental and numerical results presented a similar wave formation process. Dalrymple et al. (2002) studied the over-topping flow on deck, using a moving solid boundary to model a flap wave generator. The separated flow after wave impact on a platform deck was simulated, but the velocity profile did not match well with the experimental results,

due to the low particle resolution.

Gomez-Gesteira et al. (2005) further studied the green water over-topping under extreme waves. The wave profiles and flow separation after over-topping were modelled properly and similar to the experimental results.

Landrini et al. (2007) conducted the simulation of the propagation of near-shore bores generated by a piston wave-maker. The evolution of the breaking bores running onto a beach was investigated in detail. The flow patterns after the breaking flows were also presented and discussed.

Antuono et al. (2011) studied the generation and propagation of the regular and transient gravity waves in a basin. The tank walls and the wave maker were modelled with the fixed ghost particles technique. The wave profiles were compared with the solutions of the Mixed-Eulerian–Lagrangian method and a ideal agreement was achieved. The maximum particle space used to accurately reproduce gravity waves was analyzed and discussed in detail.

#### **1.2.2.4 Wave-body interactions**

Following the applications of the SPH method in water waves, a lot of work has been conducted to study wave-body interactions. Naito and Sueyoshi (2002) first applied the particle method to wave-body interaction problems. In this work, the Moving Particle Semi-implicit (MPS) method was adopted to simulate two-dimensional motions of a ship section with opening in waves, and flooding problems were also involved. This work proved the feasibility of the SPH method in ship-wave interactions. Since the wave-body interactions required a high resolution, Omidvar et al. (2012) used a SPH model with variable particle mass distributions. To improve the accuracy of the simulations, smaller particles were distributed near the floating body. The case studied was waves generated by the heave motion of a semi-immersed cylinder interacting

with a fixed cylinder. The calculated wave profiles showed good agreement with the experimental data, while the hydrodynamic forces on the fixed cylinder showed a noticeable difference.

This algorithm was further developed to solve three-dimensional wave-body interaction problems in Omidvar et al. (2013). In this paper, a heaving energy converter in waves was employed to validate this numerical tool. The waves were generated by a piston wave-maker. The float had six degrees of freedom in waves. The motions of the float evaluated were similar to test results in low frequency waves and less similar in high frequency waves.

Bouscasse et al. (2013) developed a two-dimensional solver employing the fixed ghost particle method to model the solid conditions. The momentum exchange method was employed to evaluate the global loads on the floating bodies. A rigid dolphin model with arbitrary solid boundary shapes was used to validate this solver. The interaction of a floating box with a group of waves was also investigated. The numerical and experimental results properly matched.

Various engineering problems were also investigated with the SPH method. Le Touze et al. (2010) conducted the three-dimensional SPH simulations to study two types of ship flooding problems. One was the deck flooding while the ship interacted with surface waves, and the other was the ship flooding after a collision happened. The water height on deck, the water height in the ship and the motions of the ship were compared with the experimental results, and good agreements were reached.

Rafiee et al. (2013) simulated the wave interactions with a wave energy converter using the Godunov SPH method with a RANS  $k-\varepsilon$  model. The time history of the pressure measured on the bottom of the tank and the wave-excited moment on the energy converter matched well with the experimental results.

Ulrich and Rung (2012) developed a multi-physics SPH model to study the water-

soil-body interactions. Three engineering examples included the installation of a gravity foundation, jacket launching from a floating platform and the propeller interactions with the hull and soil. These works proved the feasibility of the SPH method in complex multi-phase problems.

Shibata et al. (2012) used a three-dimensional Moving Particle Semi-implicit (MPS) solver to model a numerical wave tank and study the ship motions under rough seas. The non-linear phenomena in rough seas such as shipping water phenomena were captured in the simulations, although the ship motions were less similar to the experimental data.

## **1.2.3 Major drawbacks and improvements in the SPH method**

### **1.2.3.1 Boundary conditions**

In the SPH method, the integral interpolation is based on the neighbour fluid particles within the kernel support, which is a zone bounded by a circle in 2-D or a sphere in 3-D. When the kernel support is truncated by the boundary surfaces, enforcing the boundary conditions and numerical stability of the simulations can be difficult.

Free-surface boundary conditions have to be enforced in the simulations of free-surface flows. In the early stage, the free-surface conditions were considered as self-satisfied (Monaghan (1994)). However, the incomplete kernel domain truncated by free-surfaces has always been an unclear point in the SPH method. Bonet and Lok (1999) proposed two discretized formulations of the continuity equation and the momentum equations, which conserve the linear and angular momentums and stabilize the simulations of the free-surface flows. Colagrossi et al. (2009) proved these formulations can enforce the free-surface conditions in a weak way.

Solid boundary conditions play a significant role in the simulation of wall-bounded

flows. When the SPH method was first applied to the free-surface flows, a repellent force technique was proposed by Monaghan (1994). In this method, when fluid particles are close to the solid boundary, a repellent force will act on the fluid particles. Monaghan and Kajtar (2009) improved this method to effectively model the boundaries with arbitrary shapes. Although this method can easily model the fixed or moving solid boundaries, the oscillations of the particles near solid boundaries can introduce high-frequency noise into the pressure field.

The ghost particles method is another popular way to build the solid boundary conditions. The ghost particle method was first proposed by Colagrossi and Landrini (2003) for free-slip boundary conditions in the simulation of interfacial flows using the SPH method. Based on this work, Marrone et al. (2011) proposed a fixed ghost particle method, which is stable, time-saving, and can model the complex geometries.

### **1.2.3.2 High frequency noise in pressure field**

Although a wide range of the applications to free-surface flows have been conducted, the SPH method has always suffered from high frequency noise in the predicted pressure. Several techniques have been proposed to overcome this problem.

Since the pressure field is directly determined by the density field, a lot of work has been conducted to smooth the density field. Colagrossi and Landrini (2003) introduced a density reinitialization procedure based on the moving least square interpolation. Molteni and Colagrossi (2009) added a diffusive term into the continuity equation, as the artificial viscosity to the continuity equation. Antuono et al. (2010) proposed a system of equations with diffusive terms in continuity and energy equations. These methods reduce the high frequency noises in the pressure field.

Since the pressure noise can be easily excited in the weakly compressible SPH method, another approach, assuming the fluid is incompressible, has been adopted to

address the pressure problem. Cummins and Rudman (1999) proposed a projection method to enforce the incompressibility of the fluid. Shao and Lo-Edmond (2003) presented an incompressible method using prediction-correction fractional steps without enforcing the incompressibility in the prediction step. Instead of solving a pressure Poisson equation for a divergence-free velocity field, Ellero et al. (2007) used Lagrangian multipliers to enforce the incompressibility. The incompressible SPH scheme has to detect the particles on the free surface to enforce the dynamic boundary conditions on the free surface. The procedure of detection can be extremely complex and time-consuming in three dimensional simulations. Different free surface detection techniques have been proposed. Haque and Dilts (2007) created a three dimensional boundary detection method using a set of overlapping spheres to present the boundaries in particle systems. Marrone et al. (2010) proposed a fast detection method for both two-dimensional and three-dimensional simulations using a level-set function.

Anisotropic spatial distributions of the fluid particles also contribute the pressure noise and numerical instability. Since the fluid isotropic transport follows the trajectory of the fluid flow, it is difficult to guarantee that the fluid particles are always in an isotropic distribution. The particle shift technique was first proposed by Xu et al. (2009) to address the numerical instability caused by the anisotropic distribution in the incompressible SPH method with the projection-based pressure and velocity coupling. In their method, particles are slightly shifted across streamlines to avoid spacing distortion and clustering of particles. Lind et al. (2012) generalized the particle shifting method of Xu et al. (2009) to prevent highly anisotropic distributions and the onset of numerical instability. Sun et al. (2017) introduced the particle shift technique in the weakly compressible SPH method. A correction to the particle shifting technique was made to accurately detect the free surface particles and to evaluate the normal to the free surface for particles inside the free surface regions.

In the SPH method, it is unclear how to perform the particle shift procedure to rearrange the fluid particles near the free surface since this technique relies on the neighbour particles in a complete kernel support. In this thesis, a treatment for the particles near the free surface was proposed and adopted. A layer of background particles was placed along the free surface to improve the particle shift technique. The details of this algorithm will be explained in the next chapter.

### **1.2.3.3 Viscosity and numerical instability**

In the SPH method, the viscous term is usually replaced by an artificial viscous term to simplify the SPH algorithm and also to stabilize the simulations. The artificial viscous term was first proposed by Gingold and Monaghan (1982) to decrease the oscillations in shock problems. This term was further improved by Monaghan and Gingold (1983). Monaghan (1994) used this viscous term to evaluate both shear and bulk viscosity stabilizing the simulations. In the SPH method, the second derivatives could not be evaluated correctly even in a lightly anisotropic distribution of particles, which is the main reason why the real viscous term can not be employed. Takeda et al. (1994) used an anti-symmetrized viscous term to avoid the influence of particle distribution on the approximation of the second derivatives, and accurate results of the viscous flows with low Reynold number were obtained.

Tensile instability is typically troublesome in the particle technique, especially when it is applied to solid mechanics. It is an unphysical phenomena that particles cluster together when negative pressure appears. Morris (1996) conducted a stability analysis of the SPH method and proved that the Gaussian kernel can guarantee better stability. Monaghan (2000) proved that instability could be removed by an artificial pressure term, which was a repulsive force used to prevent clustering and guaranteed the tensile stability.

## 1.3 Overview

The objectives of this thesis are to simulate the interactions between breaking free-surface flows and solid structures and to improve the evaluation of hydrodynamic loads using SPH. A numerical program has been developed based on the weakly compressible SPH method involving an artificial viscous term and a diffusive term. To avoid a highly anisotropic particle distribution and its influence on the pressure predictions, a particle shift technique was adopted. As an improvement, a layer of background points along the free surface was introduced to address the challenge in applying the particle shifting technique to particles close to the free surface. The improved method was validated for a dam-break flow, the water entry of a wedge and a sloshing flow. Sensitivity studies were performed to examine the effects of the particle spacing and the time step on the solutions. The predicted free surfaces and the impact loads were compared with published experimental data and other numerical results.

Chapter 1 reviews the development of the SPH method and its application in the problems of free surface flows and fluid-structure interactions. The major drawbacks and related improvements in the SPH method are also discussed in detail.

Chapter 2 derives the SPH equations from the Euler equation with a weakly compressible assumption and a specialized equation of state. The boundary conditions and several numerical implementations are explained. An improved particle shift technique with a layer of background points along the free surface is introduced and presented in detail.

Chapter 3 presents several cases to validate the present SPH method with the improved particle shift technique. These cases include a dam-break flow, the water entry of a wedge and a sloshing flow.

Chapter 4 concludes the present work and discusses possible future work.

# Chapter 2

## Mathematical Formulation

### 2.1 Governing Equations

In this thesis, it is assumed that the fluid is inviscid, weakly-compressible and isotropic. The flow evolution is governed by conservation laws of mass and momentum. All the formulations are presented in the Lagrangian framework.

#### 2.1.1 Equations of Momentum

The equations of momentum establish the relationship between the forces acting on a fluid particle and its acceleration. The equations of momentum of inviscid fluid, which are also called Euler equations, in the Lagrangian framework state:

$$\frac{D\mathbf{u}}{Dt} = \mathbf{g} - \frac{1}{\rho}\nabla p \quad (2.1)$$

where  $\mathbf{g}$  denotes the gravitational acceleration,  $p$  and  $\rho$  is the pressure and the density of the fluid particle, respectively.  $\mathbf{u}$  is the fluid velocity defined as:

$$\frac{D\mathbf{r}}{Dt} = \mathbf{u} \quad (2.2)$$

$\mathbf{r}$  denotes the position of a fluid particle. The time history of  $\mathbf{r}$  is the trajectory of each fluid particle.

In the fluid flows governed by the Euler equations, the evolution of fluid particles is dominated by the pressure gradient and the external forces. Although it is assumed that the fluid is inviscid, an artificial viscous term will be used in the equations of momentum. This term affects the for numerical stability of the solution and is described in the following section.

### 2.1.2 Continuity Equation and Equation of State

The continuity equation, which represents the conservation of mass, can be expressed as follows:

$$\frac{D\rho}{Dt} = -\rho\nabla \cdot (\mathbf{u}) \quad (2.3)$$

where  $\rho$  is the density of the fluid particle, and  $\mathbf{u}$  is the velocity of the fluid particle. Eq. 2.3 illustrates that the density change rate of fluid particle depends on the divergence of the velocity field.

Assuming the fluid is weakly-compressible, Monaghan (1994) proposed an equation of state, which states that the pressure on a fluid particle is a single-value function of the density:

$$p = c^2(\rho - \rho_0) \quad (2.4)$$

where  $\rho_0$  is the initial density of the fluid particle, and  $c$  is the speed of sound, which

should be lower than the real speed of sound in order to avoid extremely small time steps in simulations. Entropy has a large influence on the pressure field of gas, but it is generally negligible for liquid.

The continuity equation can evaluate the rate of change of density of a fluid particle, which determines the density field of the fluid using the following equation:

$$\rho = \rho^* + \frac{D\rho}{Dt}\delta t \quad (2.5)$$

where  $\delta t$  is the time step, and  $\rho^*$  denote the density of the particle at last time step.

The pressure field of the fluid is directly determined by the density field through Eq. 2.4. The equations of momentum evaluate the acceleration of the fluid particles based on the pressure field, and then the velocity and displacement of the fluid particles can be derived as follows:

$$\mathbf{u} = \mathbf{u}^* + \frac{D\mathbf{u}}{Dt}\delta t \quad (2.6)$$

and

$$\mathbf{r} = \mathbf{r}^* + \mathbf{u}\delta t \quad (2.7)$$

where  $\mathbf{u}^*$  and  $\mathbf{r}^*$  denote the velocity and position of the particle at last time step.

## 2.2 SPH Method

### 2.2.1 Integral Interpolation

In the SPH method, the principal basis is using a convolution integral over the fluid domain to interpolate the spatial function. The value of a generic function,  $f(\mathbf{r})$  can

be interpolated as follows:

$$\langle f \rangle(\mathbf{r}) = \int_{\Omega} f(\mathbf{r}') W(\mathbf{r} - \mathbf{r}', h) dV' \quad (2.8)$$

where  $dV'$  is the volume of a differential element,  $\mathbf{r}'$  denotes the position of the differential element,  $W$  is a weight function called smoothing function or kernel, and  $h$  is the characteristic length, which determines the shape of the smoothing function.  $h$  is set between 1.01 to 1.34 times the particle spacing in this work. The smoothing function is a bell-shaped function and its value tends to zero in the region far away from the reference particle as shown in Figure 2.1. In other words, the smoothing function only has non-zero value within the kernel support, and only the particles within the kernel support are considered as neighbour particles. The radius of kernel support is called the smoothing length,  $R$ , which is 3 times  $h$  in practice.

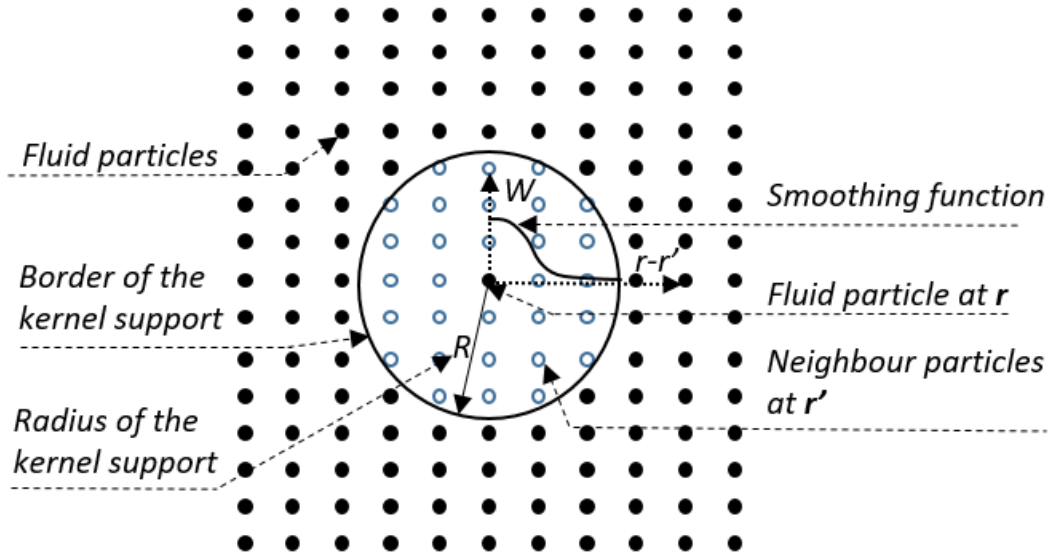


Figure 2.1: Smoothing kernel

Eq. 2.8 can exactly reproduce  $f(\mathbf{r})$  if the smoothing function is a delta function. For example, the Gaussian function with different characteristic lengths  $h$  is plotted

in Figure 2.2, the shapes of the smoothing function become sharper when  $h$  decreases from 1.5 to 0.2. If the  $h$  tends to zero, smoothing functions will approach the delta function.

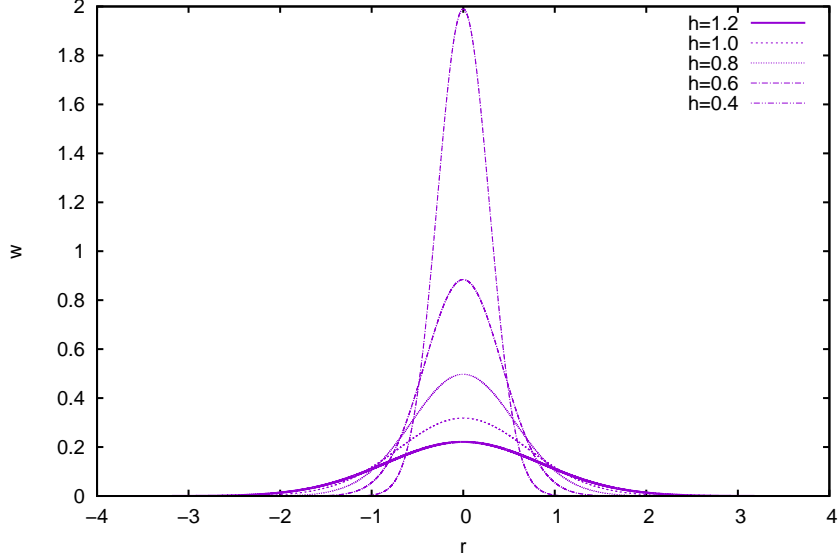


Figure 2.2: Gaussian kernel function

Substituting  $f(\mathbf{r}')$  with  $\nabla f(\mathbf{r}')$  in Eq. 2.8, the gradient of a generic function can be approximated in a similar way:

$$\langle \nabla f \rangle(\mathbf{r}) = \int_{\Omega} \nabla f(\mathbf{r}') W(\mathbf{r} - \mathbf{r}', h) dV' \quad (2.9)$$

where  $\nabla f(\mathbf{r}')$  denotes the gradient of  $f$  at  $\mathbf{r}'$ . Integrating by parts, Eq. 2.9 becomes:

$$\langle \nabla f \rangle(\mathbf{r}) = \int_{\Omega} f(\mathbf{r}') \nabla W(\mathbf{r} - \mathbf{r}', h) dV' + \int_{\partial\Omega} f(\mathbf{r}') W(\mathbf{r} - \mathbf{r}', h) \mathbf{n}' dS' \quad (2.10)$$

where  $\partial\Omega$  denotes the boundary of kernel support  $\Omega$ , and  $\mathbf{n}'$  is its unit normal vector. For  $\nabla W(\mathbf{r} - \mathbf{r}')$  and  $W(\mathbf{r} - \mathbf{r}')$ , the origin of the local coordinate system of the kernel is placed on  $\mathbf{r}'$ .

Because  $W$  is a bell-shape function equal to zero on the boundary of a complete

kernel support  $\Omega$ , the surface integral in Eq. 2.10 is equal to zero when  $\Omega$  is immersed in fluid. Consequently, Eq. 2.10 becomes:

$$\langle \nabla f \rangle(\mathbf{r}) = \int_{\Omega} f(\mathbf{r}') \nabla W(\mathbf{r} - \mathbf{r}', h) dV' \quad (2.11)$$

When  $\Omega$  is truncated by the boundary surfaces as shown in Figure 2.3, the surface integral term cannot be ignored. The surface integral needs the explicit information of the boundary surfaces, including the free surface, which can make the simulation complex and unstable. In order to force the surface integral to equal zero, a ghost particle technique is used to build the solid boundaries, which can supplement the incomplete kernel support truncated by the boundary surface. This technique will be addressed in the section 2.3.2. If the kernel support is truncated by the free surface, it is difficult to supplement the incomplete support with particles. This problem has been one of the most well-known challenges in the SPH method. A detailed discussion about the influence of the free surface on the differential operators,  $\nabla p$  and  $\nabla \cdot \mathbf{v}$ , will be presented in the section 2.2.2 and section 2.3.1.

## 2.2.2 Integral Interpolation of Differential Operators

In the governing equations,  $\nabla p$  and  $\nabla \cdot \mathbf{v}$  are the differential operators to be approximated in each time step. With the presence of the free surface, the corrected integral interpolation formulations of the differential operators were proposed by Bonet and Lok (1999) to improve the simulation results by neglecting the surface integral. These forms are the most popular formulations used in the SPH algorithm. In this thesis, they are employed as follows:

$$\langle \nabla \cdot \mathbf{u} \rangle(\mathbf{r}) = \int_{\Omega} [\mathbf{u}(\mathbf{r}') - \mathbf{u}(\mathbf{r})] \nabla W(\mathbf{r} - \mathbf{r}', h) dV' \quad (2.12)$$

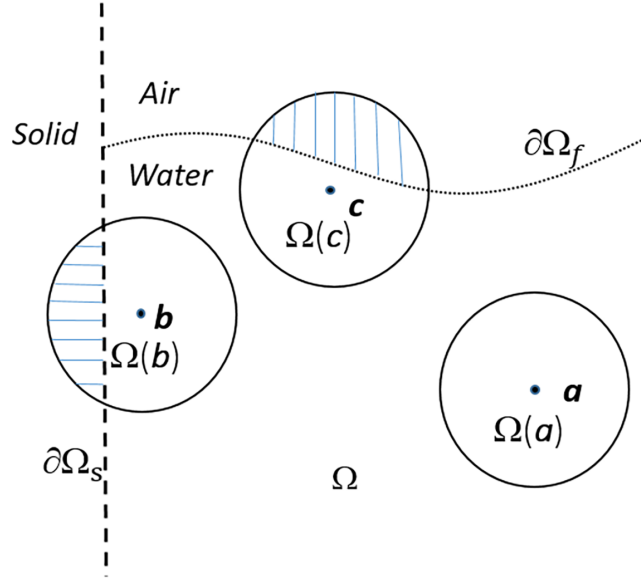


Figure 2.3: Incomplete kernels truncated by boundary surfaces

$$\langle \nabla p \rangle(\mathbf{r}) = \int_{\Omega} [p(\mathbf{r}') + p(\mathbf{r})] \nabla W(\mathbf{r} - \mathbf{r}', h) dV' \quad (2.13)$$

where  $\mathbf{v}$  is the velocity of the particle and  $p$  is the pressure of the particle. These formulations allow the surface integral to be neglected and also maintain the conservation of momentum in the SPH formulations (Colagrossi et al. (2009)).

### 2.2.3 Standard SPH Equations

Introducing smoothed differential operators into Eq. 2.1 and Eq. 2.3, the smoothed forms of the SPH equations are given below:

$$\begin{aligned}
\frac{D\rho}{Dt} &= -\rho \int_{\Omega} [\mathbf{u}(\mathbf{r}') - \mathbf{u}(\mathbf{r})] \nabla W(\mathbf{r} - \mathbf{r}', h) dV' \\
p &= c^2(\rho - \rho_0) \\
\frac{D\mathbf{u}}{Dt} &= \mathbf{g} - \frac{1}{\rho} \int_{\Omega} [p(\mathbf{r}') + p(\mathbf{r})] \nabla W(\mathbf{r} - \mathbf{r}', h) dV' \\
\frac{D\mathbf{r}}{Dt} &= \mathbf{u}
\end{aligned} \tag{2.14}$$

Substituting the convolution integral with summation to Eq. 2.14,

$$\int_{\Omega} \nabla W(\mathbf{r} - \mathbf{r}', h) dV' = \sum_i \nabla W_{ij} V_j \tag{2.15}$$

leads to the discretized SPH equations:

$$\begin{aligned}
\frac{D\rho_i}{Dt} &= -\rho_i \sum_j (\mathbf{u}_j - \mathbf{u}_i) \nabla_i W_{ij} V_j \\
p_i &= c^2(\rho_i - \rho_0) \\
\frac{D\mathbf{u}_i}{Dt} &= \mathbf{g} - \frac{1}{\rho_i} \sum_j (p_j + p_i) \nabla_i W_{ij} V_j \\
\frac{D\mathbf{r}_i}{Dt} &= \mathbf{u}_i
\end{aligned} \tag{2.16}$$

where the subscript  $j$  denotes the particles within the kernel support of particle  $i$ ,  $\nabla_i W_{ij}$  denotes the gradient at particle  $i$  of the smoothing kernel at particle  $j$ ,  $V_i$  is defined as the volume of particle  $i$ , and the mass of particle  $i$  is  $m_i = \rho_i V_i$ . In practice, it is assumed that the mass of the fluid particle is constant in the simulation, and the density of the fluid particle changes in the rate defined in Eq. 2.3. Consequently, the volume of the fluid particle changes with its density as  $V_i = m_i / \rho_i$ .

For those new to the SPH method, it is sometimes hard to understand what the fluid particle really is. A fluid particle is not a dot, but its position is represented by its initial volume center. Although the volume of each fluid particle is known and changes with relative motions of the neighbour particles, the shape of the fluid particle is arbitrary and not of interest.

## 2.2.4 SPH Equations with numerical diffusive and viscous terms

Two main drawbacks of the SPH algorithm are numerical instability and high frequency noise in pressure due to the discontinuity in the density field. In this work, an artificial viscous term proposed by Monaghan (1994) was used in the equations of momentum to improve the numerical stability. A numerical diffusive term proposed by Antuono et al. (2010) was also added into the continuity equation to allow a small exchange of mass between neighbour particles. The SPH equations with the artificial viscous term and the numerical diffusive term are expressed by:

$$\begin{aligned}
 \frac{D\rho_i}{Dt} &= -\rho_i \sum_j (\mathbf{u}_j - \mathbf{u}_i) \nabla_i W_{ij} V_j + \delta hc \sum_j \boldsymbol{\psi}_{ij} \cdot \nabla_i W_{ij} V_j \\
 p_i &= c^2(\rho_i - \rho_0) \\
 \frac{D\mathbf{u}_i}{Dt} &= \mathbf{g} - \frac{1}{\rho_i} \sum_j (p_j + p_i) \nabla_i W_{ij} V_j + \alpha hc \sum_j \boldsymbol{\pi}_{ij} \nabla_i W_{ij} V_j \\
 \frac{D\mathbf{r}_i}{Dt} &= \mathbf{u}_i
 \end{aligned} \tag{2.17}$$

where  $\alpha$  is the artificial viscous coefficient,  $\delta$  is the diffusive coefficient. In practice,  $\alpha$  is set between 0.05 and 0.2, and  $\delta$  is set to 0.3.  $\boldsymbol{\pi}_{ij} = (\mathbf{u}_j - \mathbf{u}_i) \frac{\mathbf{r}_{ji}}{|\mathbf{r}_{ji}|^2}$ ,  $\boldsymbol{\psi}_{ij} = 2(\rho_j - \rho_i) \frac{\mathbf{r}_{ji}}{|\mathbf{r}_{ji}|^2} - [\langle \nabla \rho \rangle_i^L + \langle \nabla \rho \rangle_j^L]$ ,  $\mathbf{r}_{ji}$  is the displacement from particle  $i$  to  $j$ , and

the normalized density gradient  $\langle \nabla \rho \rangle^L$  is defined as follows:

$$\begin{aligned} \langle \nabla \rho_a \rangle^L &= \sum_b (\rho_b - \rho_a) \mathbf{L}_a \nabla_a W_{ab} dV_b, \\ \mathbf{L}_a &= \left[ \sum_b (\mathbf{r}_b - \mathbf{r}_a) \otimes \nabla_a W_{ab} dV_b \right]^{-1} \end{aligned} \quad (2.18)$$

where  $a$  denotes the particle of interest,  $b$  denotes its neighbour particles, and  $\otimes$  denotes tensor product.

## 2.3 Boundary Conditions

### 2.3.1 Free-surface Boundary Condition

On the free surface, the kinematic condition and the dynamic condition must be satisfied. The kinematic condition means that the particles initially located on the free surface will remain on the surface, i.e.,

$$\mathbf{u} \cdot \mathbf{n}_F = \mathbf{V}_{\partial\Omega_F} \cdot \mathbf{n}_F \quad \forall \mathbf{x} \in \Omega_F \quad (2.19)$$

where  $\mathbf{n}_F$  is the normal vector of the free surface,  $\mathbf{u}$  is the velocity of the fluid particle, and  $\mathbf{V}_{\partial\Omega_F}$  is the velocity of this moving boundary. This condition can be implicitly satisfied due to the Lagrangian characteristic of the SPH method (Colagrossi et al. (2009)).

The dynamic free-surface boundary condition means that the pressure along the free surface would be equal to the external pressure  $p_e$  if surface tension was ignored, i.e.,

$$p(\mathbf{x}) = p_e \quad \forall \mathbf{x} \in \Omega_F \quad (2.20)$$

Practically, the external pressure is usually set to zero. Colagrossi et al. (2009)

proved that the dynamic free-surface boundary condition is satisfied in a weak way when using the specified smoothed differential operators defined in Eq. 2.12 and Eq. 2.13.

### 2.3.2 Solid Boundary Condition

In this thesis, a fixed ghost particle method proposed by Marrone et al. (2011) was adopted to satisfy the solid boundary condition. In this method, a layer of ghost particles, which were used to supplement the truncation of the incomplete kernel support, were placed along the solid boundaries. The ghost particles were fixed to the solid boundary, and their quantities of physical properties were mirrored from the interpolation points in fluid domain.

According to Marrone et al. (2011), the algorithm for the generation of the ghost particles is performed with the following steps: At first, the solid boundary profile is approximately represented with surface nodes with a distance equal to the fluid particle spacing. Secondly, the normal vector  $\mathbf{n}$  and the tangent vector  $\mathbf{t}$  are defined for each node, where the normal vectors point outwards from the fluid domain and the tangent vectors are defined through the right-hand law: the cross product of  $\mathbf{n}$  and  $\mathbf{t}$  is positive. Then, the ghost particles are generated by reproducing the boundary nodes in the normal direction with a distance equal to the fluid particle spacing. Figure 2.4 presents the finished distribution of the ghost particles. Figure 2.5 shows the arrangement of the interpolation points, which are generated with a procedure similar to the ghost particles.

As shown in Figure 2.6, physical quantities of the interpolation points are accurately interpolated from the neighbour fluid particles with the Moving Least-Squares (MLS) method (Fries and Matthies (2003)). For example, the pressure of a ghost

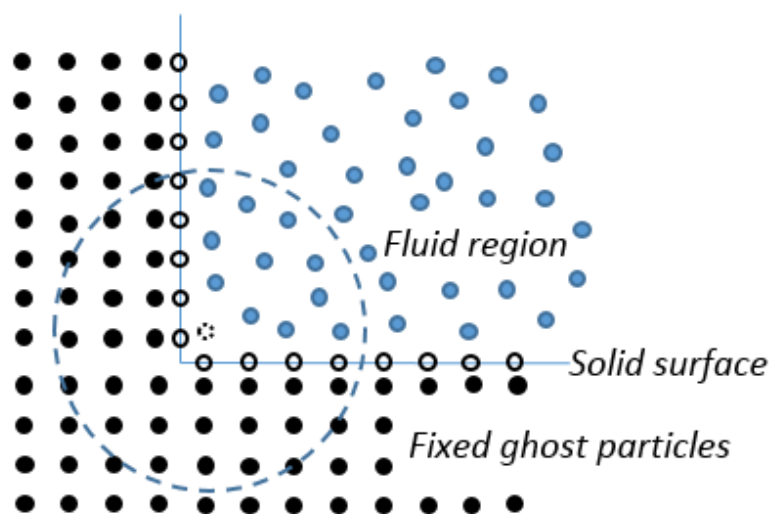


Figure 2.4: Sketch of an incomplete kernel supplemented by fixed ghost particles

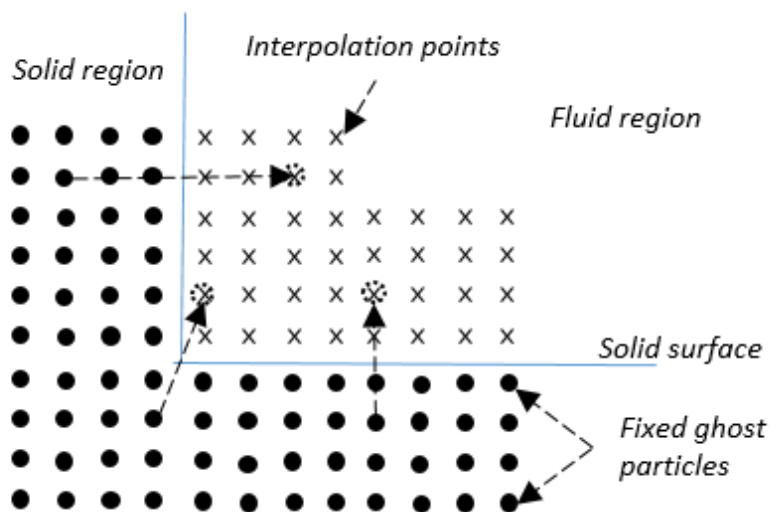


Figure 2.5: Interpolation points of fixed ghost particles

particle is evaluated as follows:

$$p_g = \sum_j p_j W^{\text{MLS}}(\mathbf{r}_j) dV_j + 2d\rho\mathbf{g} \cdot \mathbf{n} \quad (2.21)$$

where  $\mathbf{g}$  is gravitational acceleration,  $\mathbf{n}$  is the normal vector of the surface node, and  $d$  is the distance between the ghost particle and its interpolation point. The Moving Least-Squares kernel  $W^{\text{MLS}}$  is defined as:

$$\begin{aligned} W^{\text{MLS}}(\mathbf{r}_j) &= \mathbf{M}_i^{-1} \mathbf{e}_1 \cdot \mathbf{b}_{ij} W(\mathbf{r}_j) \\ \mathbf{b}_{ij}^T &= [1, (x_j - x_i), (y_j - y_i), (z_j - z_i)]; \mathbf{e}_1^T = [1, 0, 0, 0] \\ \mathbf{M}_i &= \sum_j \mathbf{b}_{ij} \otimes \mathbf{b}_{ij} W(\mathbf{r}_j) dV_j \end{aligned} \quad (2.22)$$

where  $\otimes$  denotes the tensor product, and  $(x_i, y_i, z_i)$  and  $(x_j, y_j, z_j)$  is the coordinate of particle  $i$  and particle  $j$ , respectively.

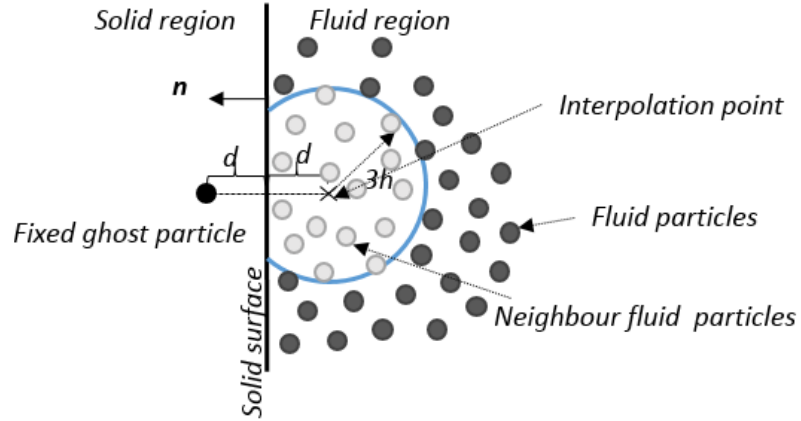


Figure 2.6: Sketch of the interpolation of the fixed ghost particle

When moving solid boundaries are involved in the simulations, the evaluation of the velocity of the ghost particles,  $\mathbf{u}_g$ , needs special attention. As presented in Figure 2.7,  $\mathbf{u}_g$  depends on the velocity of the solid surface nodes,  $\mathbf{u}_b$ , and the velocity

evaluated on the interpolation point,  $\mathbf{u}_i$ . According to Colagrossi and Landrini (2003), the no-slip boundary conditions can be described as follows:

$$\begin{aligned}\mathbf{u}_g \cdot \mathbf{n} &= 2\mathbf{u}_b \cdot \mathbf{n} - \mathbf{u}_i \cdot \mathbf{n} \\ \mathbf{u}_g \cdot \mathbf{t} &= \mathbf{u}_i \cdot \mathbf{t}\end{aligned}\tag{2.23}$$

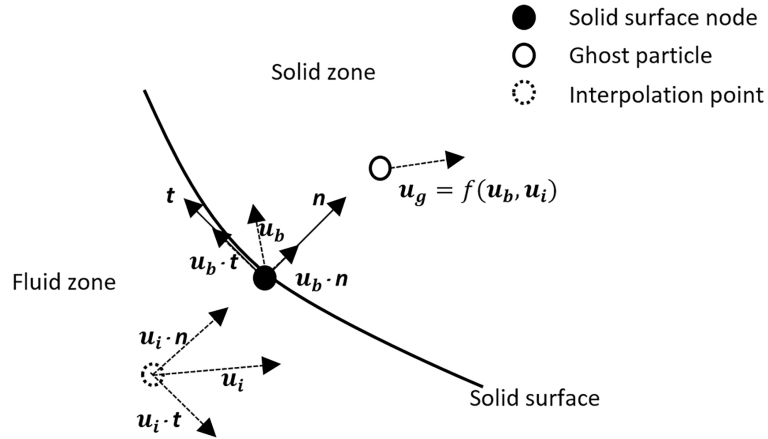


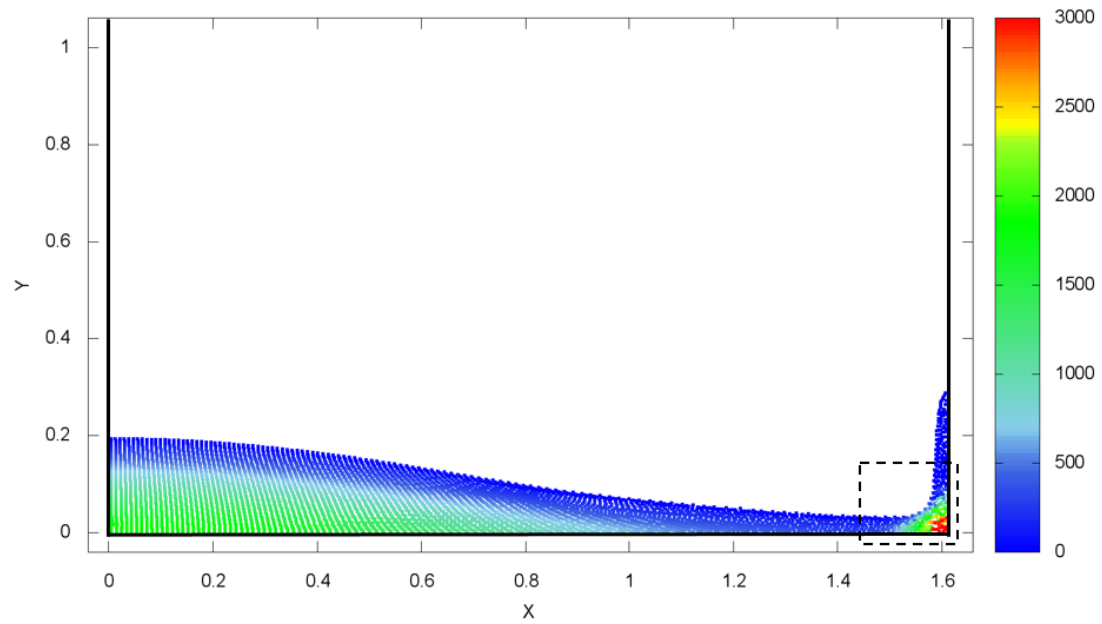
Figure 2.7: Sketch of the velocity of the fixed ghost particle

## 2.4 Particle shift technique

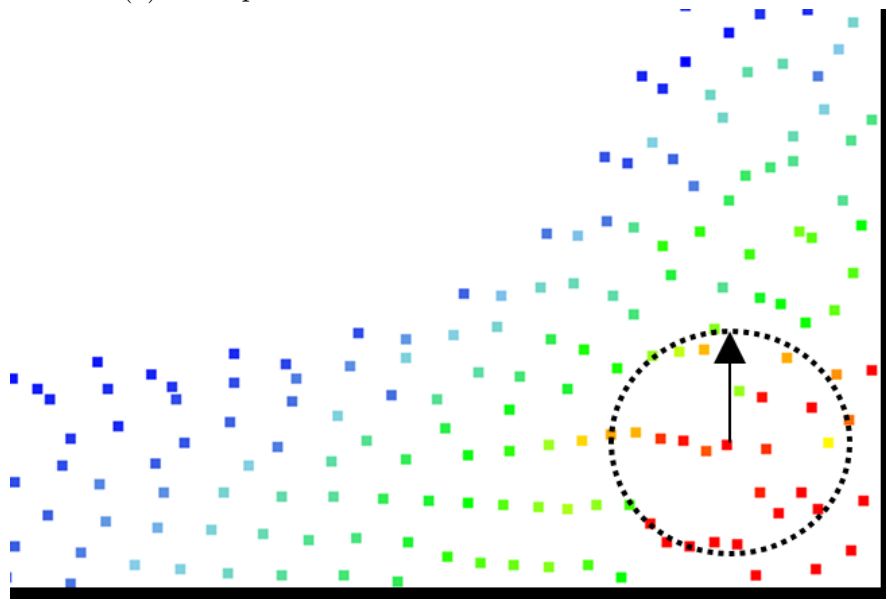
### 2.4.1 Disordered particles distribution problem

The spatial distribution of fluid particles is a key element in SPH simulations. Since the fluid particles move following the evolution of the fluid flow, it is difficult to guarantee a isotropic distribution of the fluid particles at any time step, especially in fluid zones with high velocity gradients. Figure 2.8 presents an anisotropic distribution of the fluid particles in the wall corner for a dam breaking flow case.

In order to investigate the influence of anisotropic particle distribution on the interpolation procedure in the SPH method, Colagrossi et al. (2009) proposed an



(a) A snapshot of the simulation of the dam-break flow



(b) Enlarged snapshot of the corner area under violent impact

Figure 2.8: Anisotropic particle distribution in dam-break flow

identity  $\nabla\Gamma$  to evaluate the level of the approximation error of the differential operators defined in Eq. 2.12 and Eq. 2.13.  $\nabla\Gamma$  can be interpreted as the approximation of the gradient of a constant field and derived as follows:

$$\int_{\Omega} f_0 \nabla W(\mathbf{r} - \mathbf{r}', h) dV' = f_0 \sum_j \nabla W_{ij} \frac{m_j}{\rho_j} = f_0 \nabla\Gamma \quad (2.24)$$

where  $f_0$  is a constant spatial function. According to Eq. 2.24,  $\nabla\Gamma$  becomes:

$$\sum_j (\nabla W_{ij} \frac{m_j}{\rho_j}) = \nabla\Gamma \quad (2.25)$$

In theory, the gradient of the constant field should be equal to zero. However, the anisotropic distribution of the fluid particles leads to a non-zero value of  $\nabla\Gamma$ , which stands for the level of approximation error of Eq. 2.12 and Eq. 2.13. In practice, the particle shift technique is employed to reduce this type of error.

## 2.4.2 Particle shift formulations

The particle shift technique was first proposed by Xu et al. (2009) to rearrange the distribution of the fluid particles in the incompressible SPH method. In the SPH algorithm, the error described in Eq. 2.25 automatically turns into a nonphysical force in Eq. 2.17 enforcing the distribution of particles to be more isotropic (Antuono et al. (2014)). Although this approach tends to decrease the level of anisotropic distribution, the particle distribution problem is still significant in the high velocity gradient zone as shown in Figure 2.8. According to the work of Sun et al. (2017), the particle shift technique was enhanced by slightly modifying the positions of particles

using the following equations:

$$\delta \mathbf{r}_i = -CFL \cdot Ma \cdot (2h)^2 \cdot \sum_j \nabla_i W_{ij} \frac{2m_j}{\rho_j + \rho_i} \quad (2.26)$$

$$\mathbf{r}_i^* = \mathbf{r}_i + \delta \mathbf{r}_i \quad (2.27)$$

where  $\mathbf{r}_i^*$  is the new position of the particle,  $\delta \mathbf{r}_i$  is the shift distance,  $CFL$  is the Courant number,  $h$  is the character length of smoothing function, and  $Ma$  is the Mach number.  $Ma$  is set to 0.1 in this work.

### 2.4.3 Background particles along the free surface

For a particle near the free surface, its kernel support is incomplete. In this case, the particle shift technique, which is based on the distribution of the neighbour particles in a full kernel support, becomes ineffective and even can lead to numerical instability.

Several solutions have been proposed to address this difficulty near the free surface. According to Sun et al. (2017) and Khayyer et al. (2017), in the area near the free surface, the shifting distance of the fluid particles was forced to be equal to zero in the normal direction of the free surface in different ways.

In this thesis, a new treatment was applied to address this problem. The incomplete kernel support is compensated by a layer of background or virtual particles along the boundary surface. This treatment follows the idea of using the fixed ghost particles to compensate the kernel truncation near solid boundaries. Note that the virtual particles do not interact with the fluid particles or affect the evolution of the fluid flows.

In the algorithm, two main steps are required to distribute virtual particles along the boundary surfaces. In the first step, the initial background particles are uniformly distributed in the computational domain at the beginning of the simulation by using

the same particle spacing as that for the fluid particles as shown Figure 2.9. In the second step, some background particles along the boundary surfaces are chosen and set as active background particles to compensate the kernel support near boundary surfaces as shown in Figure 2.10. Because the free surface keeps moving, this process is carried out at each time step. The criterion for choosing the active particles is based on a summation defined in Eq. 2.28, representing the filling level of the kernel support of initial background particles.

$$\Gamma = \sum_j (W_{ij} V_j) \quad (2.28)$$

where  $i$  denotes the initial background particle,  $j$  denotes the neighbour fluid particles of the initial background particle,  $W_{ij}$  is the weight function and  $V_j$  is the volume of the fluid particle  $j$ . As shown in Figure 2.11, the fluid particle within the kernel support of the initial background particle are used to calculate  $\Gamma$ .

$$\begin{aligned} \Gamma > \Gamma_{fs} & \text{ inactive} \\ \Gamma = 0.0 & \text{ inactive} \\ 0.0 < \Gamma < \Gamma_{fs} & \text{ active} \end{aligned} \quad (2.29)$$

The criteria in Eq. 2.29 determines the status of the initial background particles. For  $0.0 < \Gamma < \Gamma_{fs}$ , the initial background particle is considered as an active background particle. When  $\Gamma > \Gamma_{fs}$ , it means that an initial background particle is immersed in fluid. When  $\Gamma = 0.0$ , it implies that the initial background particles are not within the kernel support of any fluid particle. In the current practice,  $\Gamma_{fs}$  is set to 0.40. A snapshot of the active background particles in the simulation of dam break is presented in Figure 2.12. These particles compensate the missing part of the kernel support to improve the particle shift technique near a boundary.

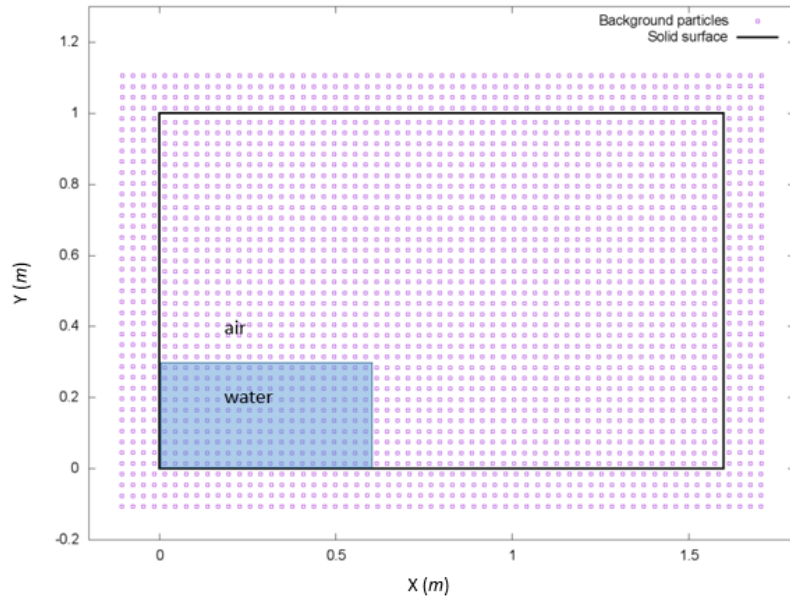


Figure 2.9: Distribution of initial background particles

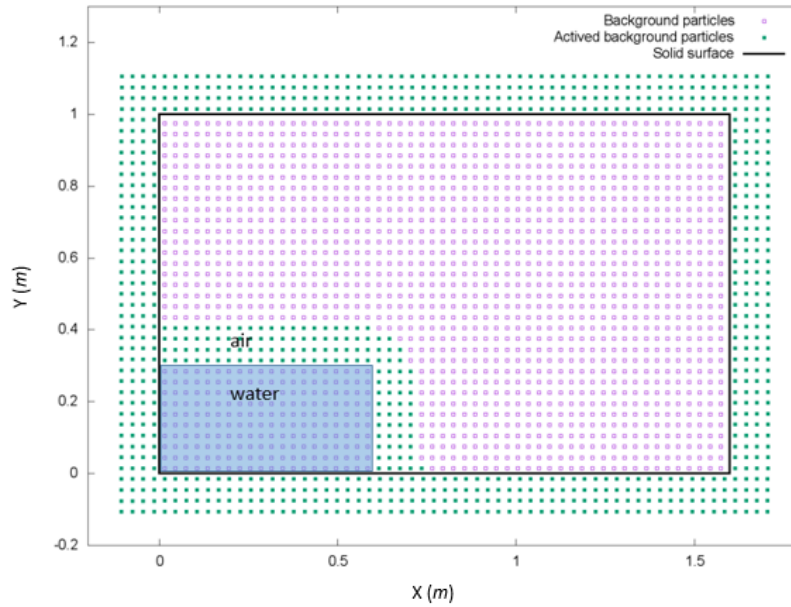


Figure 2.10: Active background particles

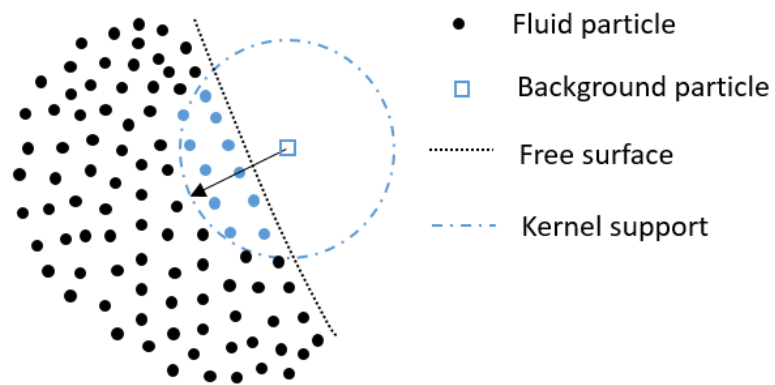


Figure 2.11: Neighbour particles of background particles

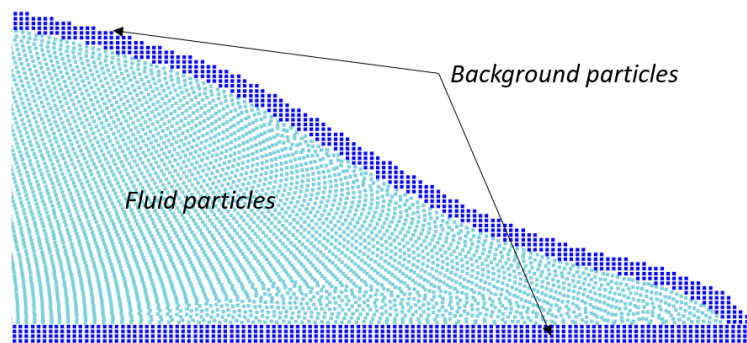


Figure 2.12: Background particles and fluid particles

## 2.5 Numerical Implementations

### 2.5.1 Gaussian Kernel

To approximate the governing equations in the simulations, a kernel function is necessary. The kernel adopted in this thesis is a renormalized Gaussian kernel proposed by Marrone (2012).

$$W(r) = \begin{cases} \frac{e^{-(r/h)^2} - C_0}{2\pi C_1} & r \leq R \\ 0 & \text{otherwise} \end{cases} \quad (2.30)$$

$$C_0 = e^{-(R/h)^2}; C_1 = \int_0^R r[e^{-(r/h)^2} - e^{-(R/h)^2}]$$

where  $r$  is the distance between two particles,  $R$  is the radius of kernel support, and  $h$  is the character length, which determines the shape of kernel function. In this thesis, the character length remains constant and equals 1.33 times particle spacing. The kernel radius equals  $3h$ , which means the number of particles within the kernel support is about 50.

### 2.5.2 Choice of time schemes

In the SPH method, the time step is mainly limited by the particle spacing, the relative speed of particles and the speed of sound used in the equation of state. Marrone (2012) proposed a formulation to evaluate the time step in each loop as follows:

$$\Delta t = CFL \min_i \left( \frac{h}{c_i + |u_i| + h \max_j |\pi_{ij}|} \right) \quad (2.31)$$

where  $\min_i$  denotes the minimum value over all the fluid particles,  $\max_j$  indicates the maximum value over the neighbour particles of the particle  $i$ , and  $CFL$  is the Courant

number determined by the time scheme adopted.  $\pi_{ij}$  is defined in Eq. 2.17, which represents the relative motion among the neighbour particles.

In this thesis, the Euler scheme proposed by Marrone (2012) was adopted, which include a predictor step and a corrector step depicted in Eq. 2.32 and Eq. 2.33, respectively.

$$\begin{aligned}
 \rho_i^{n+\frac{1}{2}} &= \rho_i^n + \Delta t E_i^n \\
 \mathbf{u}_i^{n+\frac{1}{2}} &= \mathbf{u}_i^n + \Delta t \mathbf{G}_i^n \\
 \mathbf{r}_i^{n+\frac{1}{2}} &= \mathbf{r}_i^n + \Delta t \mathbf{u}_i^n + \frac{\Delta t^2}{2} \mathbf{G}_i^n
 \end{aligned} \tag{2.32}$$

where  $n + \frac{1}{2}$  indicates the predictor step,  $\mathbf{G}$  denotes acceleration, and  $E$  is density change rate.

$$\begin{aligned}
 \rho_i^{n+1} &= \rho_i^n + \Delta t \frac{E_i^n + E_i^{n+\frac{1}{2}}}{2} \\
 \mathbf{u}_i^{n+1} &= \mathbf{u}_i^n + \Delta t \frac{\mathbf{G}_i^n + \mathbf{G}_i^{n+\frac{1}{2}}}{2} \\
 \mathbf{r}_i^{n+1} &= \mathbf{r}_i^{n+\frac{1}{2}}
 \end{aligned} \tag{2.33}$$

where  $n + 1$  indicates the corrector step. When the Euler scheme is adopted, CFL is usually set between 0.2 and 0.9, which can lead to a stable simulation in practice.

### 2.5.3 Global Forces on Floating Bodies

The evaluation of the global hydrodynamic force is key in the fluid-structure interaction problems. Generally, there are two methods to evaluate the global loads on floating bodies: the surface integral method and the momentum exchange method. The former uses a smoothing procedure to evaluate the pressure on body surface, and integrates the pressure along the surface to obtain the global forces and moments. In

contrast, the latter can be performed through a summation of the quantities already evaluated in the equations of momentum. The interactions between the solid particles and the fluid particles can be considered an exchange of momentum. Every portion of the fluid-solid interactions is summed up to evaluate the global loads.

In this thesis, the global forces,  $\mathbf{F}_S$ , were evaluated with the momentum exchange method by Bouscasse et al. (2013) as follows:

$$\mathbf{F}_S = \int_{\Omega_F} dV \int_{\Omega_S} -(p' + p) \cdot \nabla W(\mathbf{r}' - \mathbf{r}) dV' \quad (2.34)$$

where  $\Omega_F$  is the fluid domain,  $\Omega_S$  is the solid domain,  $p'$  is the pressure of the solid particles, and  $p$  is the pressure of the fluid particles. The discretized form is given by:

$$\mathbf{F}_S = \sum_j \sum_i -(p_j + p_i) \cdot \nabla_i W_{ij} V_i V_j \quad (2.35)$$

Introducing the artificial viscous term defined in Eq. 2.17, Eq. 2.35 becomes:

$$\mathbf{F}_S = \sum_j \sum_i (-(p_i + p_j) + \alpha hc \rho_0 \pi_{ij}) \cdot \nabla_i W_{ij} V_i V_j \quad (2.36)$$

where  $i$  denotes the fluid particles, the  $j$  means the solid particles,  $\alpha hc \rho_0 \pi_{ij}$  is the viscous term. Similarly, the moment on the floating body can be presented as follows:

$$\begin{aligned} \mathbf{M}_S = & \sum_j \sum_i \{ (\mathbf{r}_j - \mathbf{r}_c) \times (-p_i + \alpha hc \rho_0 \pi_{ij}/2) \nabla_i W_{ij} \\ & + (\mathbf{r}_i - \mathbf{r}_c) \times (-p_j + \alpha hc \rho_0 \pi_{ij}/2) \nabla_i W_{ij} \} V_i V_j \end{aligned} \quad (2.37)$$

where  $i$  denotes the fluid particles, the  $j$  means the solid particles,  $\mathbf{r}_c$  is the center of gravity of the body.

### 2.5.4 Equations of motion for a floating body

The motions of rigid body are governed by Newton's law of motion. The 2-D linear and angular equations of motion are given as follows:

$$\begin{aligned} M \frac{d\mathbf{V}}{dt} &= M\mathbf{g} + \mathbf{F}_s \\ I \frac{d\mathbf{\Omega}}{dt} &= \mathbf{M}_s \end{aligned} \tag{2.38}$$

where  $\mathbf{V}$  and  $\mathbf{\Omega}$  are the linear velocity at the center of gravity and angular velocity of the body, respectively,  $M$  is the mass,  $I$  is the moment of inertia of the rigid body,  $\mathbf{g}$  is the gravitational acceleration,  $\mathbf{F}_s$  and  $\mathbf{M}_s$  are the hydrodynamic force and moment acting on the rigid body, respectively.

## 2.6 Summary of the computation

A program based on the present SPH model was developed in FORTRAN. This program can deal with breaking free-surface flows and its interactions with fixed or moving rigid structures. Moreover, it can solve the problems with violent impact phenomena and evaluate the local and global impact loads. Figure 2.13 presents the detailed steps of the numerical computation.

The fluid and rigid structures are modelled with the fluid particles and the ghost solid boundary particles. The initial velocity, density, pressure of the fluid particles are set according to the initial conditions. When the simulation starts, the list of neighbour particles is created for each fluid particle. The computational domain is divided into square cells. For a particle in a cell, the surrounding particles in the neighbour cells are its potential neighbour particles. The distance between the potential neighbour particle and the particle of interest is calculated. If the distance is less than the kernel support radius, the particle would be considered as a neighbour

particle. This selecting procedure is performed in every time step. The neighbour particles of the interpolation points of the solid boundary particles are also marked in the same way. The physical quantities of every solid boundary particle are interpolated through the neighbour particles of its counterpart interpolation point. Then, the physical quantity change rates of each fluid particle are evaluated based on the neighbour particles following the SPH equations. According to the change rates of the physical field, the density, pressure, velocity and position of the fluid particles are updated. The momentum of the rigid body is evaluated through the momentum exchange between the fluid particles and the solid boundary particles. The solid boundary particles advance according to the motions of the solid boundaries. After the motions of fluid and solid particles are obtained, a loop of the simulation for one time step is finished, and a new loop will continue until the time is equal to the maximum time.

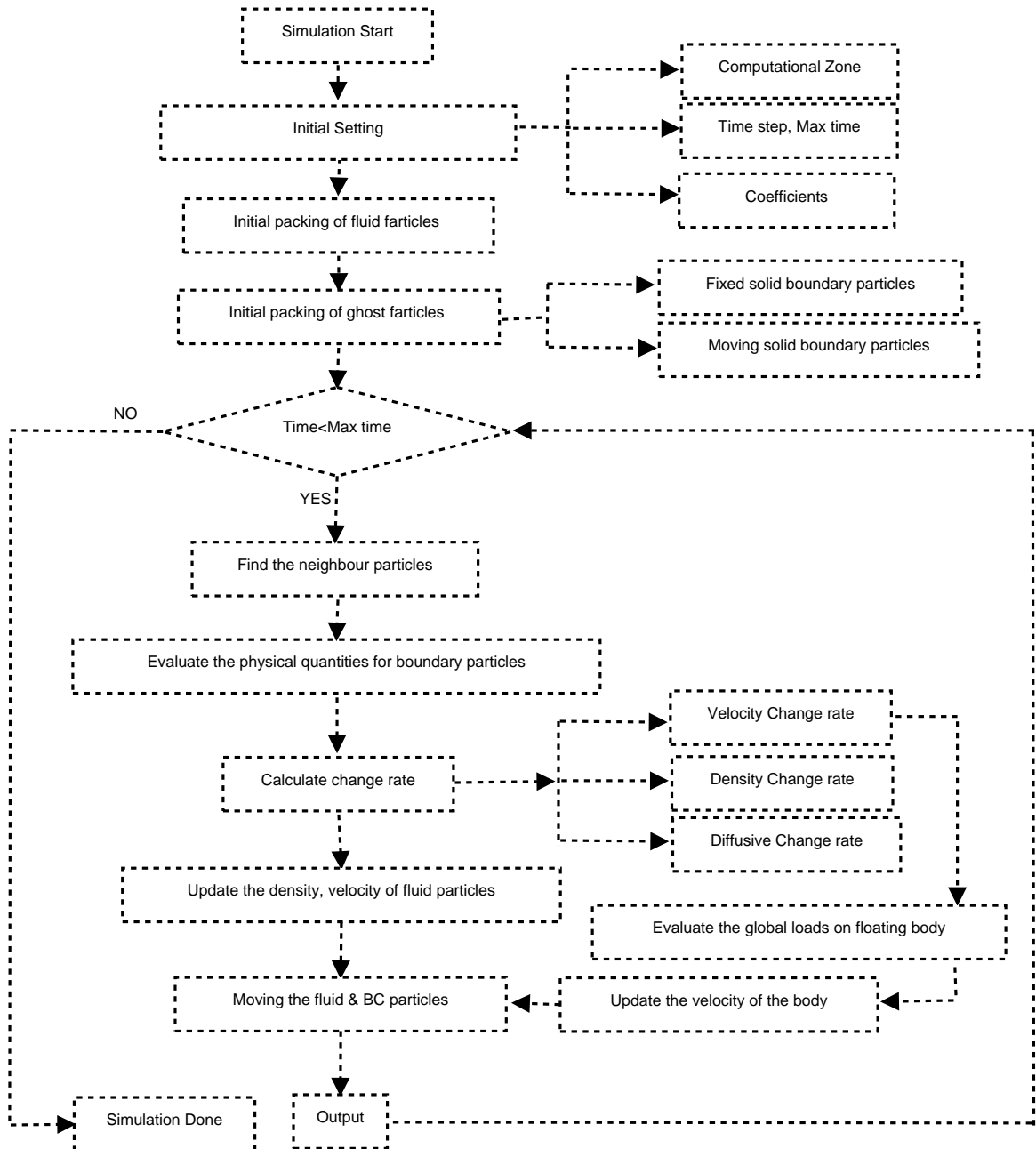


Figure 2.13: Flowchart of the numerical algorithm

# Chapter 3

## Numerical Results

In this chapter, several two-dimensional cases were conducted to validate the accuracy, feasibility and robustness of the present SPH algorithm with a particle shift technique in the free surface flows interacting with fixed or moving solid structures. These three cases include: (1) dam-break flow impacts on a vertical wall; (2) water entry of a wedge; (3) and sloshing flow excited by the roll motions.

### 3.1 Dam-break flow

#### 3.1.1 Case description

The dam-break flow is the standard test case. This case involves several complex physical phenomena including violent fluid-solid and fluid-fluid impacts, free surface breaking and fluid segments.

The simulations were according to the conditions of the experimental tests conducted by Lobovsky et al. (2014) in which a large number of test repetitions were performed to address the repeatability of the experiments. The setup of this test is illustrated in Figure 3.1. The length of the tank was  $1.6m$ . The water cube had a

height of  $0.3m$  and a length of  $0.6m$ . The points  $P_1$  and  $P_2$  represented the pressure sensors, which recorded the local pressures during the test. The vertical positions of the sensors placed on the vertical wall were  $0.003m$  and  $0.015m$ , respectively measured from the tank bottom. In the section of  $H_1$ , the time history of water height was also recorded.

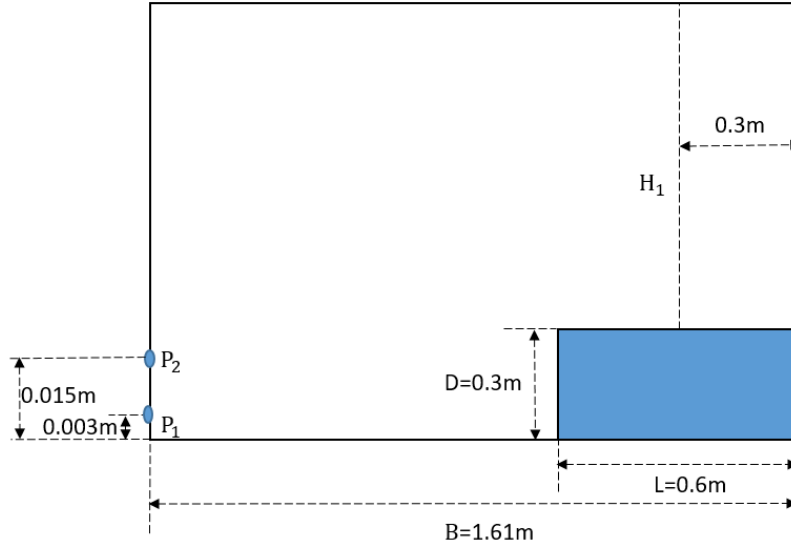


Figure 3.1: Sketch of the setup of the dam-break test

### 3.1.2 Convergence study

The convergence of the numerical solution, in terms of the impact pressure at  $P_1$ , to the particle spacing and the time step size was investigated. Three computational cases were first conducted with different particle spacing:  $0.003m$ ,  $0.002m$  and  $0.0015m$ , corresponding to 11, 250, 20, 000 and 45, 000 fluid particles, respectively. The  $CFL$  number is set to 0.6. Figure 3.2 shows that the predicted pressure converges when more particles are employed. Another three cases were then carried out with constant particle spacing,  $0.002m$ , and different  $CFL$  numbers: 0.60, 0.75 and 0.90. As shown in Figure 3.3, the numerical results are not sensitive to the time step size.

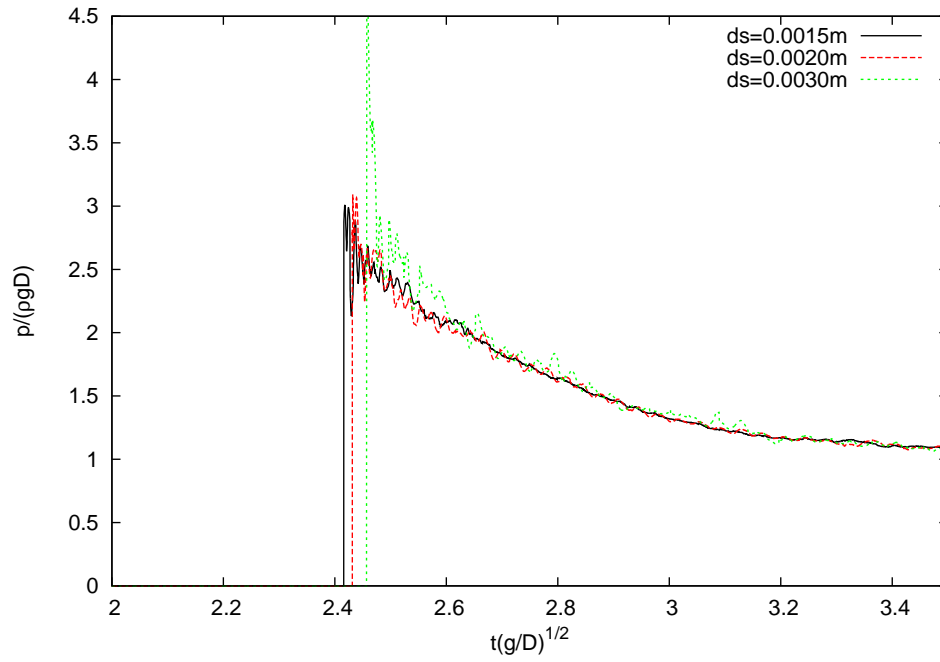


Figure 3.2: Sensitivity of the pressure on  $P_1$  to the particle spaces

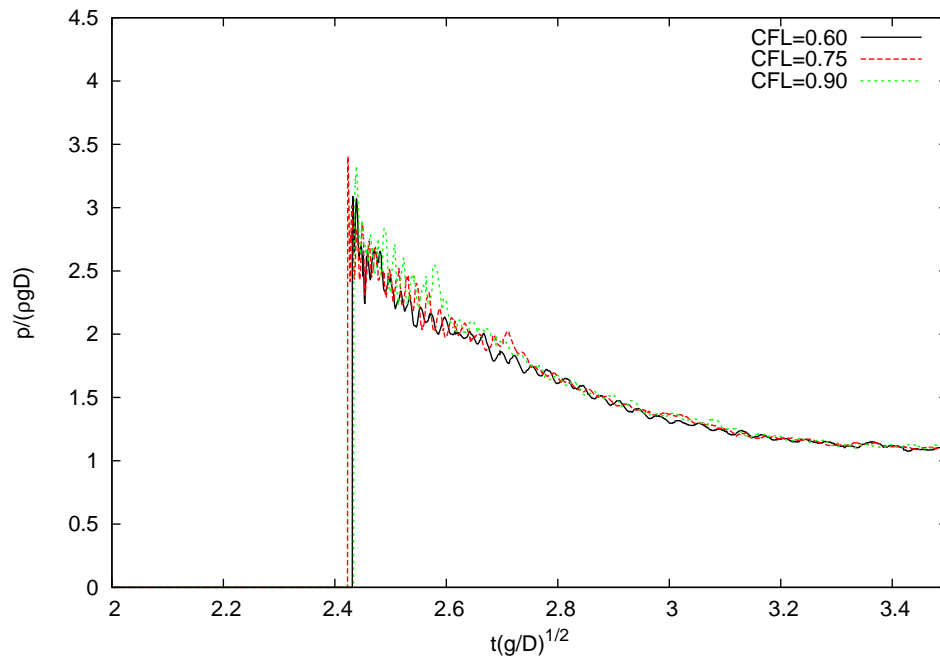


Figure 3.3: Sensitivity of the pressure on  $P_1$  to the time step sizes

### 3.1.3 Simulation results

In the simulation, the particle spacing is set to  $0.0015m$ . 45,000 fluid particles and 7,252 fixed ghost particles were employed to model the fluid flow and the solid walls of the tank. The  $CFL$  number is set to 0.6. The front of the dam-break flow and the water height measured at  $H_1$  were compared with the experimental results by Lobovsky et al. (2014) in Figures 3.4 and 3.5, respectively. Both time series agree well with the experimental results.

The time series of the pressures on  $P1$  and  $P2$  are illustrated in Figures 3.6 and 3.7. The numerical results with and without the particle shift technique are compared with the experimental results by Lobovsky et al. (2014). The predicted pressures generally agree with the experimental results. The present method with the shift technique led to smoother pressures than the original SPH model. It proves that the particle shift technique decreases the oscillations in the impact pressures. Figure 3.8 compares the particle distribution at the corner and indicates the present model gives a more uniform particle distribution than the original model. The snapshots of the flow evolution at different time instances are presented in Figures 3.9 to 3.11 and compared with the experimental photos. The predicted free surface is very similar to the experimental one.

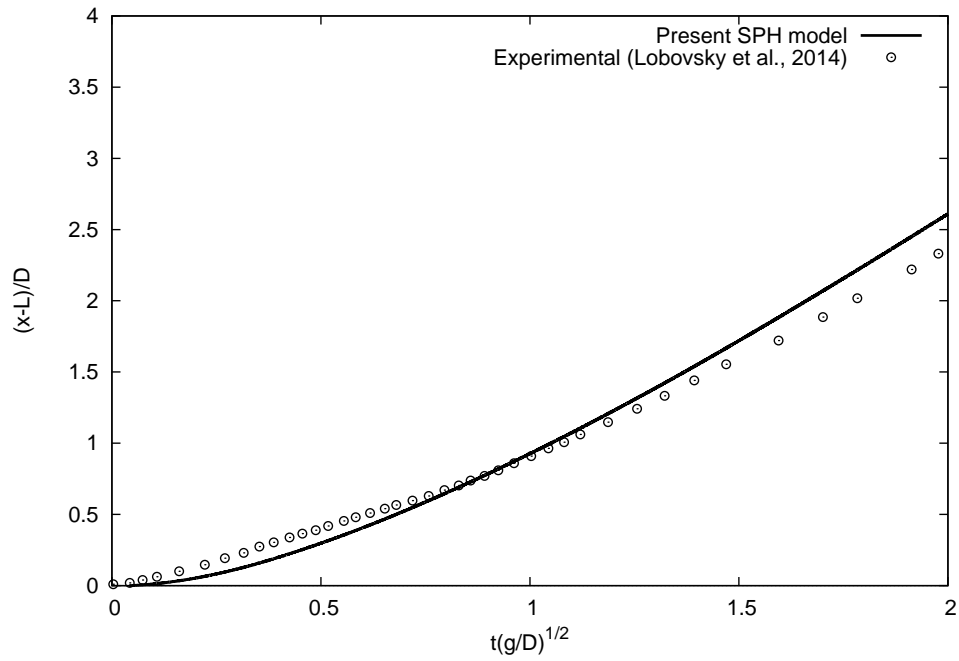


Figure 3.4: Comparison between the flow fronts measured by the simulation and experiments

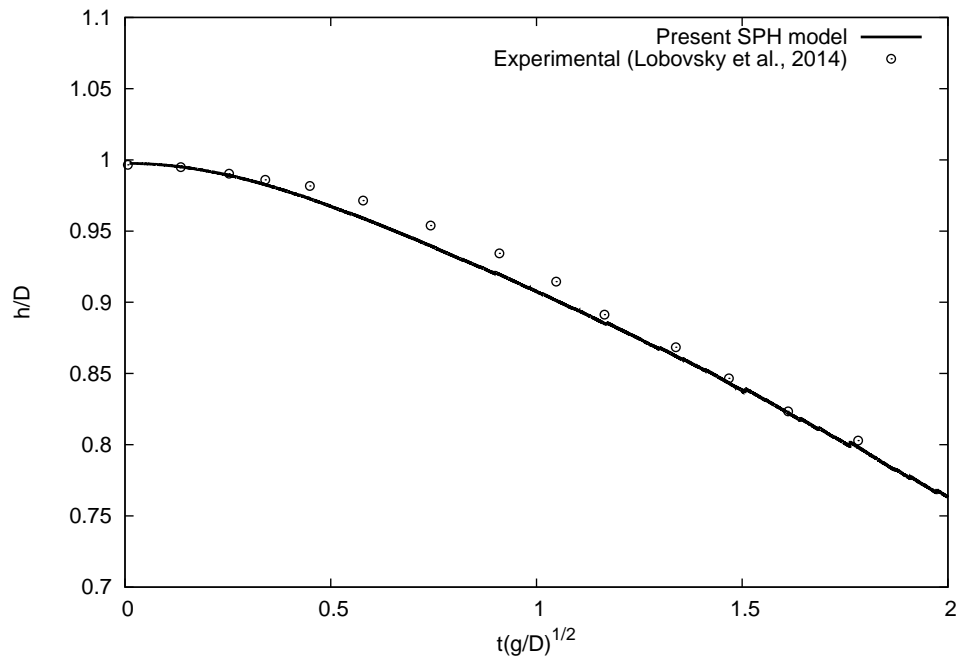


Figure 3.5: Comparison between the flow heights measured by the simulation and experiments at probe  $H_1$

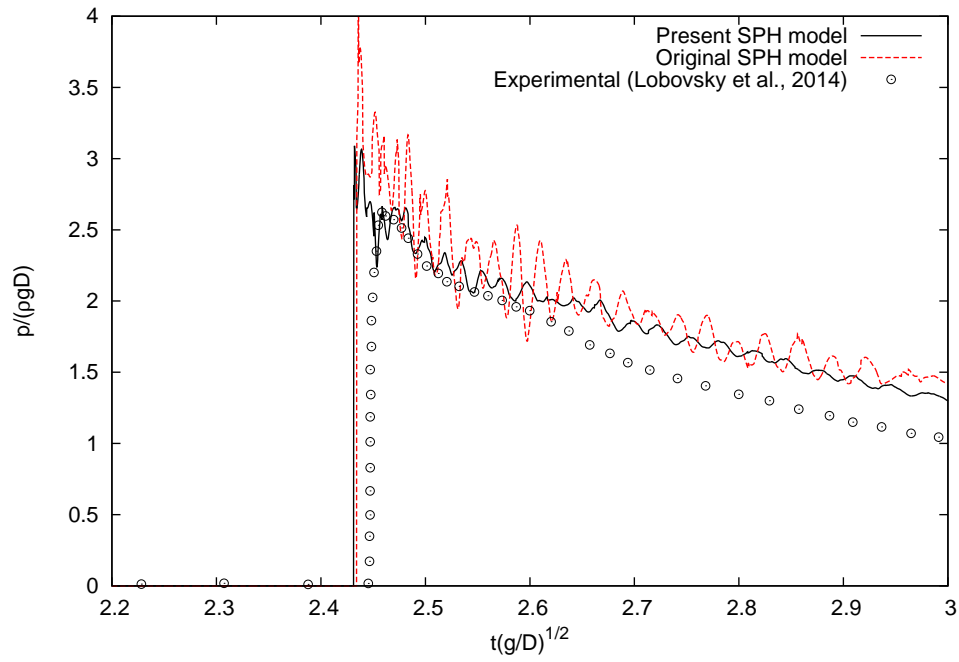


Figure 3.6: Comparison between the pressures measured at probe  $P_1$  with  $ds=0.002m$

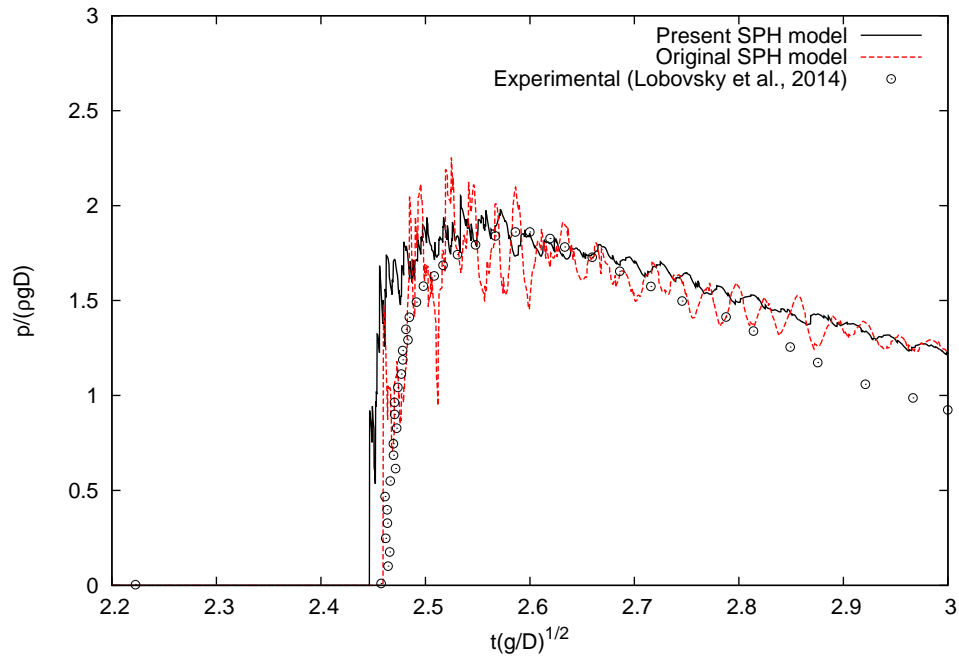


Figure 3.7: Comparison between the pressures measured at probe  $P_2$  with  $ds=0.002m$

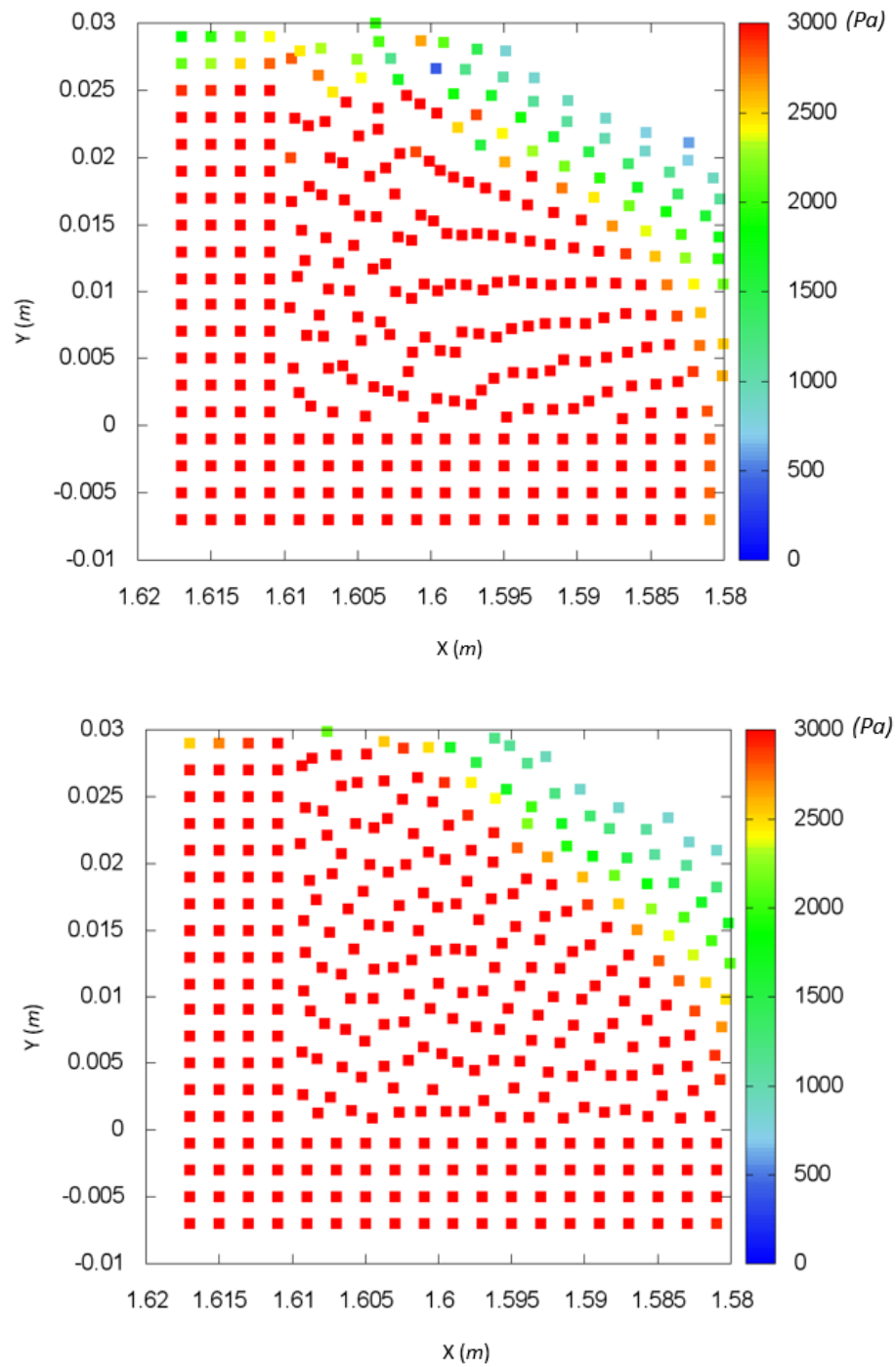


Figure 3.8: Particle distribution near pressure sensor  $P_1$  in dam-break flow by the original SPH method (top) and the present SPH method (below)

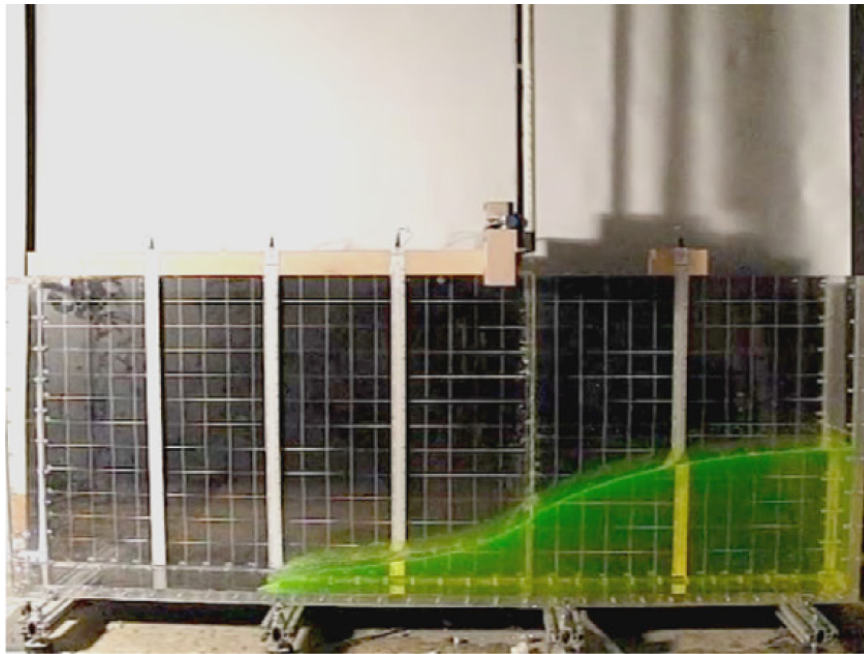
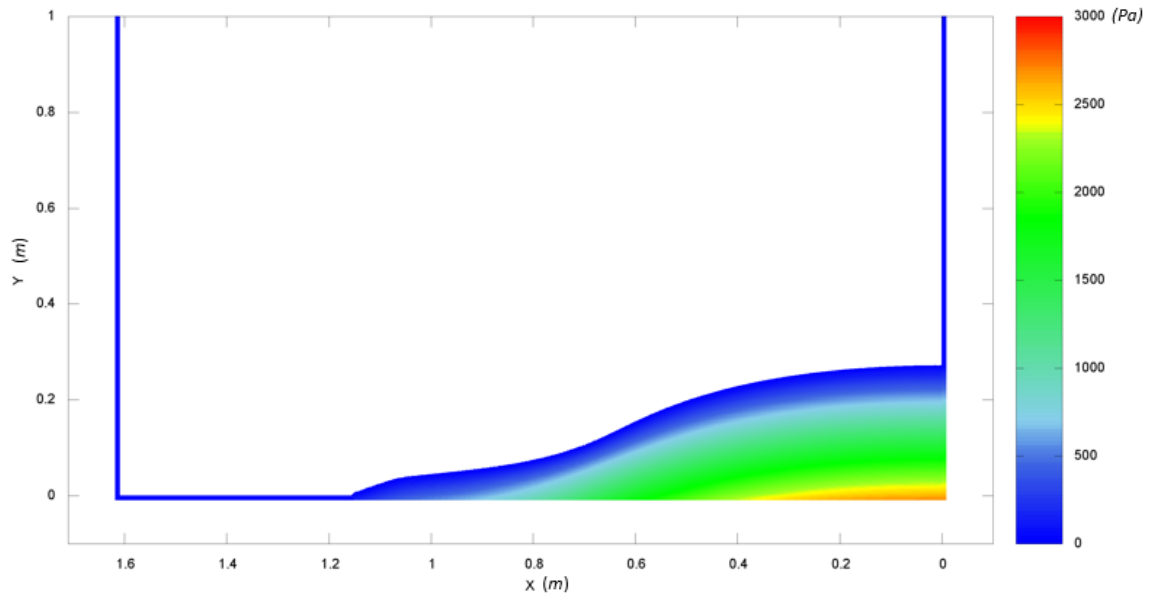


Figure 3.9: Snapshots of the evolution of the dam-break flow at  $t(g/H)^{1/2} = 1.58$

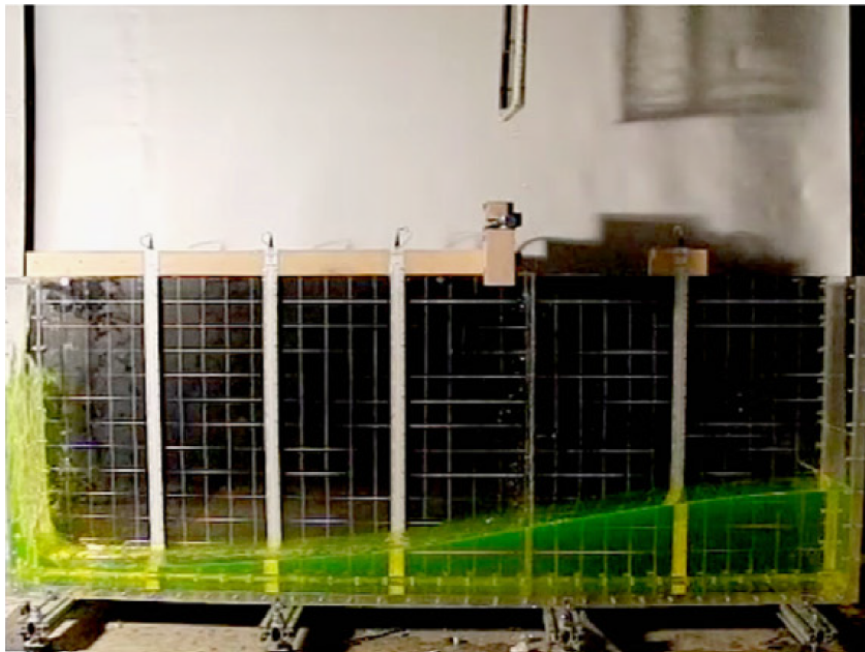
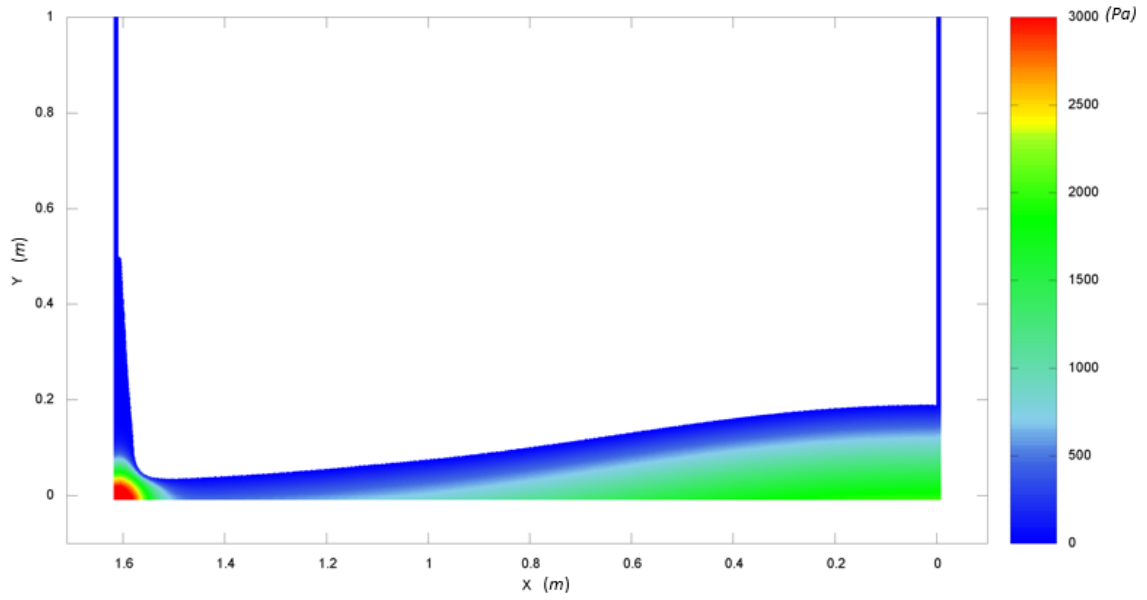


Figure 3.10: Snapshots of the evolution of the dam-break flow at  $t(g/H)^{1/2} = 3.27$

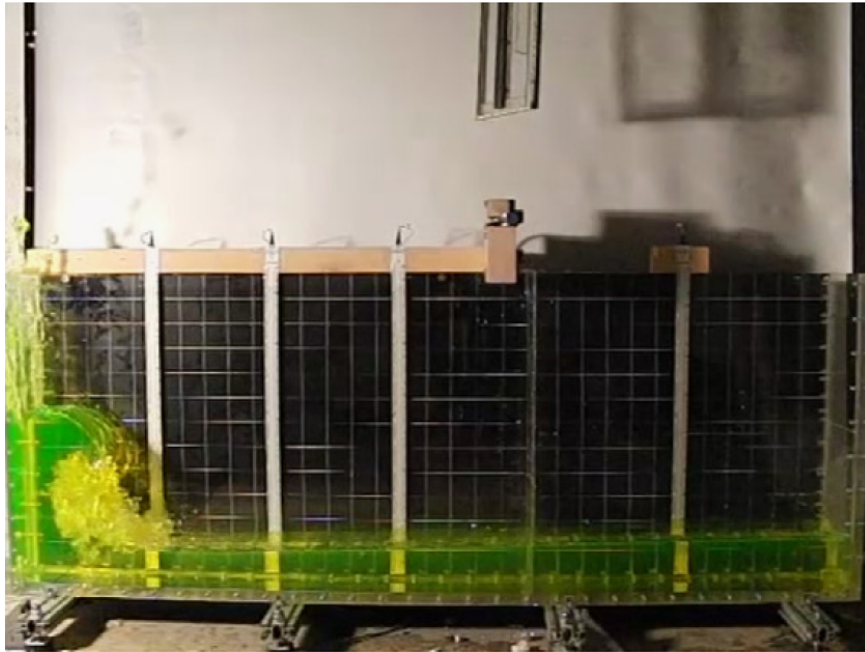
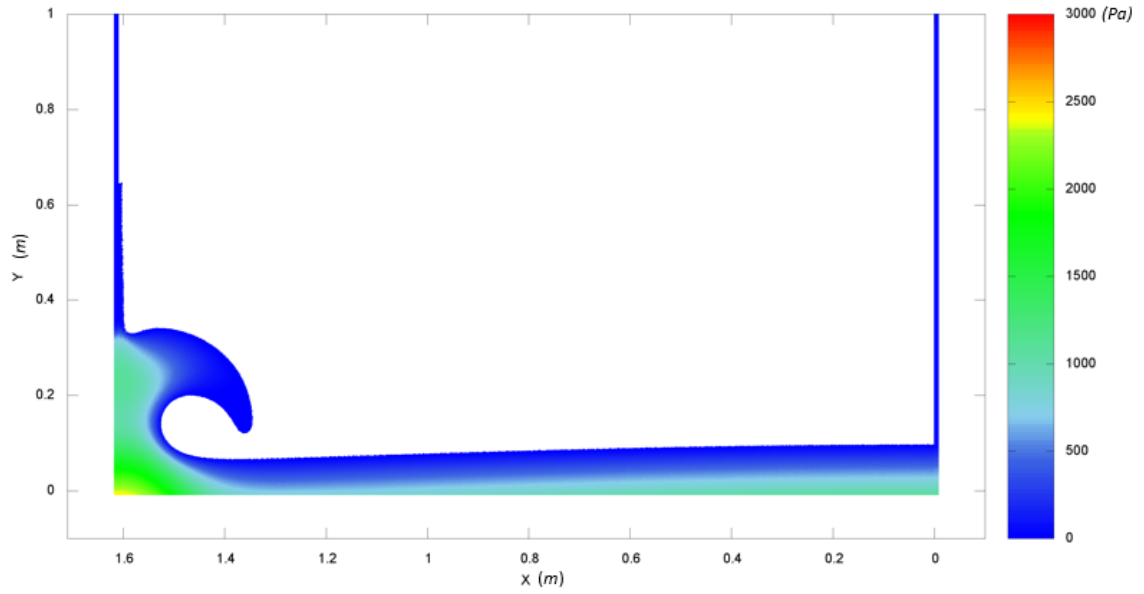


Figure 3.11: Snapshots of the evolution of the dam-break flow at  $t(g/H)^{1/2} = 5.85$

## 3.2 Water entry

The water entry of a free-fall body is another complex hydrodynamic problem with strong fluid-solid impact and breaking free surface. The local and global slamming loads were investigated in detail to validate the capability of the present SPH solver.

### 3.2.1 Case description

The water entry of a symmetric wedge was simulated and the results were compared with the experimental data by Zhao et al. (1996). The computational domain is illustrated in Figure 3.12. The deadrise angle of the wedge was  $30^\circ$ ; its width,  $B$ , was  $0.5m$ ; its drop height,  $H$ , was  $2.0m$ . The tank had a depth of  $1.0m$  and a width of  $3.0m$ . To reduce the computational cost, the simulations started at the moment when the wedge touched the water surface with an initial velocity of  $2.9m/s$ . The wedge had only one degree of freedom. As an example, Figure 3.13 shows the distribution of fluid particles and the solid ghost particles.

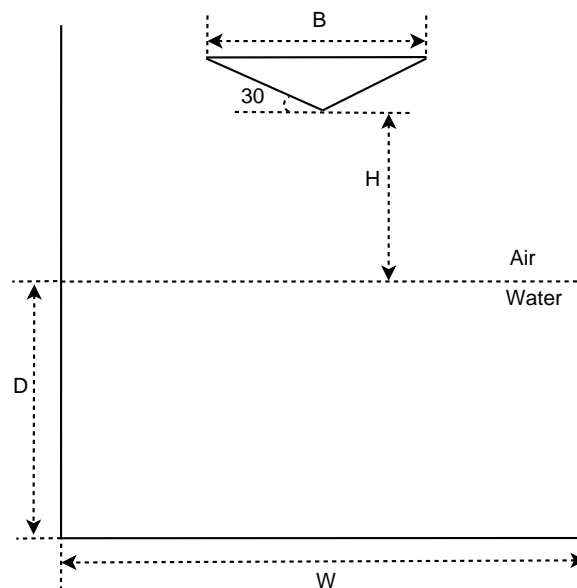


Figure 3.12: Sketch of the water entry of a wedge

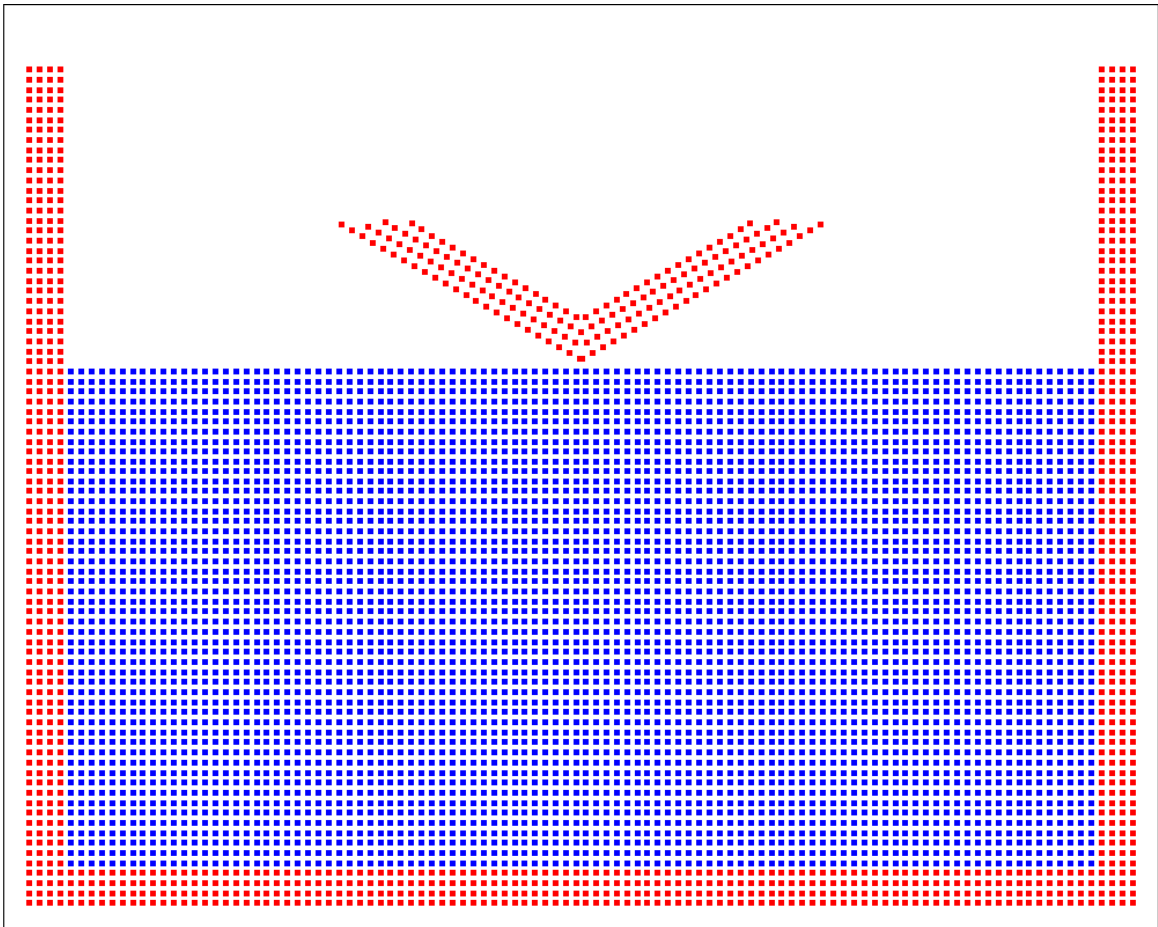


Figure 3.13: Distribution of the fluid particles and solid ghost particles

### 3.2.2 Convergence study

To investigate the convergence of the numerical solution to the particle spacing and the time step size, the hydrodynamic force on the wedge was computed using various time step sizes and particle spacings. Three cases were first conducted with a constant  $CFL$  number, 0.4, and particles spacing:  $B/100$ ,  $B/200$  and  $B/300$ , which are corresponding to 120,000, 480,000 and 1,080,000 fluid particles, respectively. Another three cases were then conducted with constant particle spacing,  $B/300$ , and different  $CFL$  numbers: 0.4, 0.6 and 0.8. As shown in Figure 3.14, the numerical solutions become smoother and converge as the particle spacing decreases. As indicated in Figure 3.15, the solutions are insensitive to the time step size.

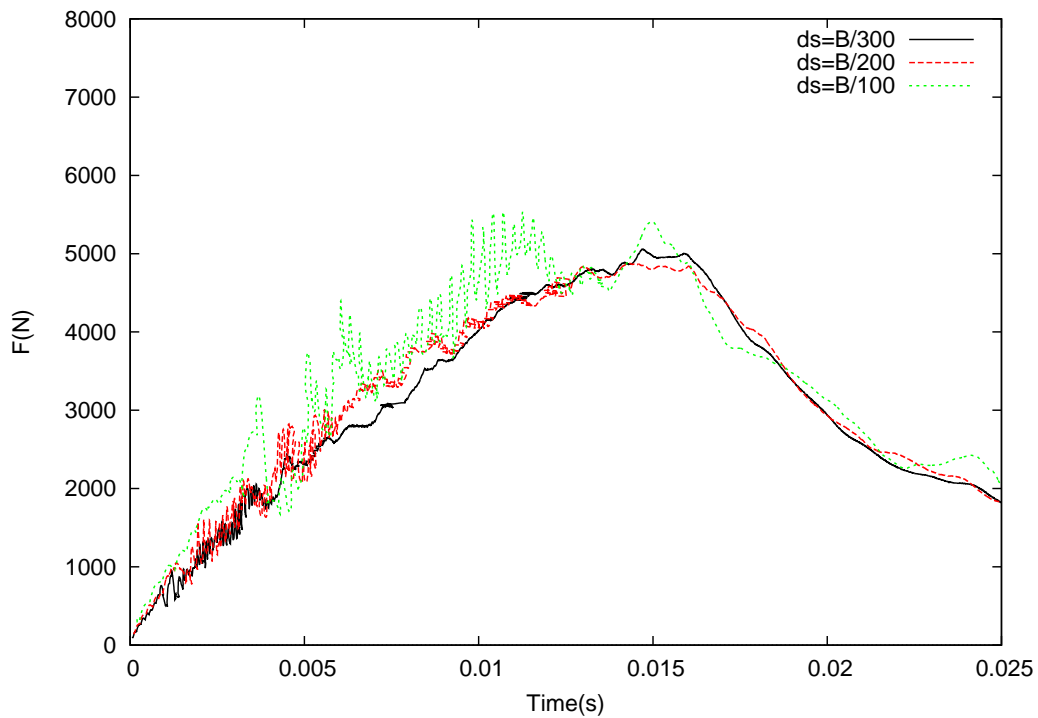


Figure 3.14: Sensitivity of the slamming force to particle spacing

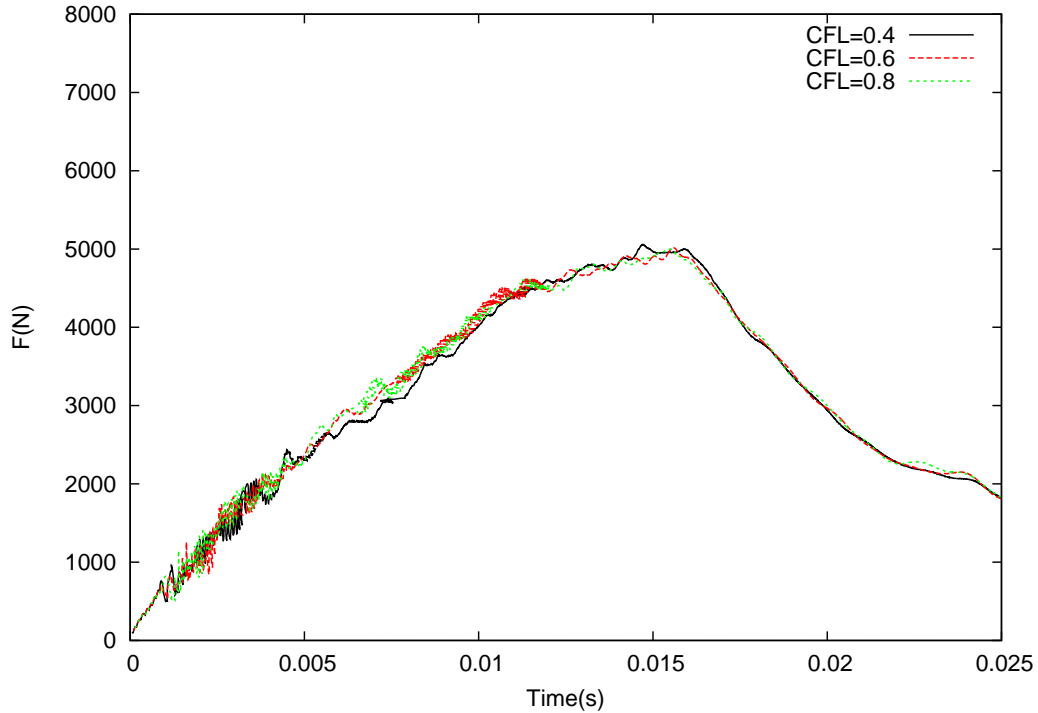


Figure 3.15: Sensitivity of the slamming force to time step size

### 3.2.3 Simulation results

In the following simulations, the particle spacing and the  $CFL$  number were set as  $B/300$  and 0.4, respectively. In total, 1,080,000 fluid particles, 10,818 fixed ghost particles and 1,192 fixed ghost particles were employed to model the fluid, the tank walls and the wedge, respectively.

The time series of the slamming force and the falling velocity of the wedge were compared with experimental results by Zhao et al. (1996). As shown in Figure 3.16, the predicted falling velocity agree well with the experimental one. The time history of the slamming force is also in a good agreement with the experimental one as shown in Figure 3.17. It is found that the particle shift technique slightly improves the prediction of the global slamming loads. In fact, the particle shift technique is aimed to improve the distribution of fluid particles and decrease the oscillations in

the pressure field. Because of the statistical features of the integral interpolation, the global loads are not sensitive to the pressure noises in the SPH simulations.

Two snapshots of the particle distribution near the free surface and the solid wedge predicted by the SPH method with and without the technique are given in Figure 3.18. A nonphysical cavity occurs at the water jet region with high velocity gradients in the snapshot by the original SPH model. The nonphysical cavity however does not appear in the snapshot predicted by the present method with the particle shift technique.

The pressure distributions on the wedge surface at different time instances, predicted by the present method, are compared with the experimental results and the fully non-linear solution based on the boundary element method by Zhao et al. (1996) in Figures 3.19 to 3.21. In these figures, the non-dimensional vertical coordinate is represented with  $Z/S$ , where  $S$  is the instantaneous draft of the wedge, and  $Z$  is the vertical coordinate on the wedge surface relative to the calm free surface. It is shown that the present method with the particle shift technique gives more stable pressure results than the original SPH model. The snapshots of the flow field are also presented in Figures 3.19 to 3.21.

A uniform distribution of particles is the basis of the prediction of the impact pressure. The particle shift technique rearranged the fluid particles to a more uniform distribution, especially near the free surface as shown in Figure 3.18, and improved the impact pressure distribution on the solid boundary.

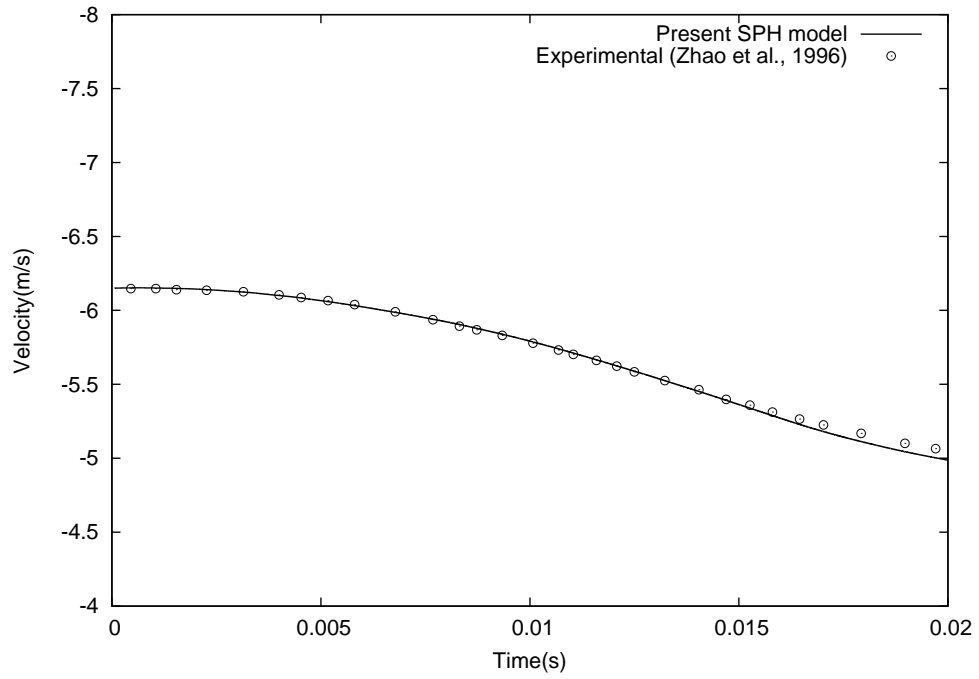


Figure 3.16: Time history of the velocity of the wedge during the drop test

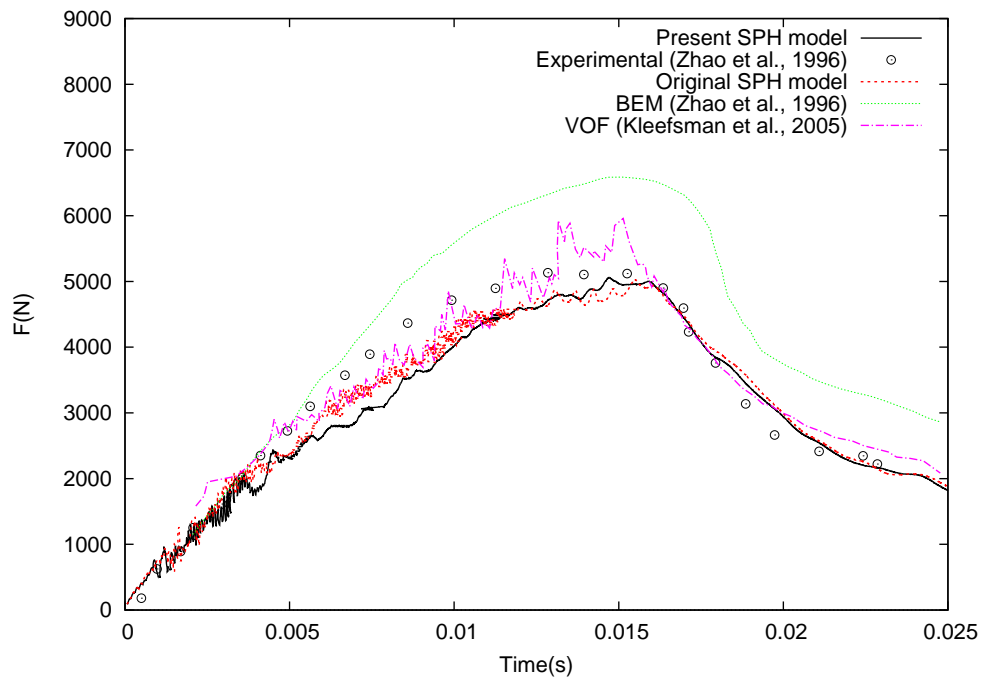


Figure 3.17: Time history of the slamming force on the wedge during the test

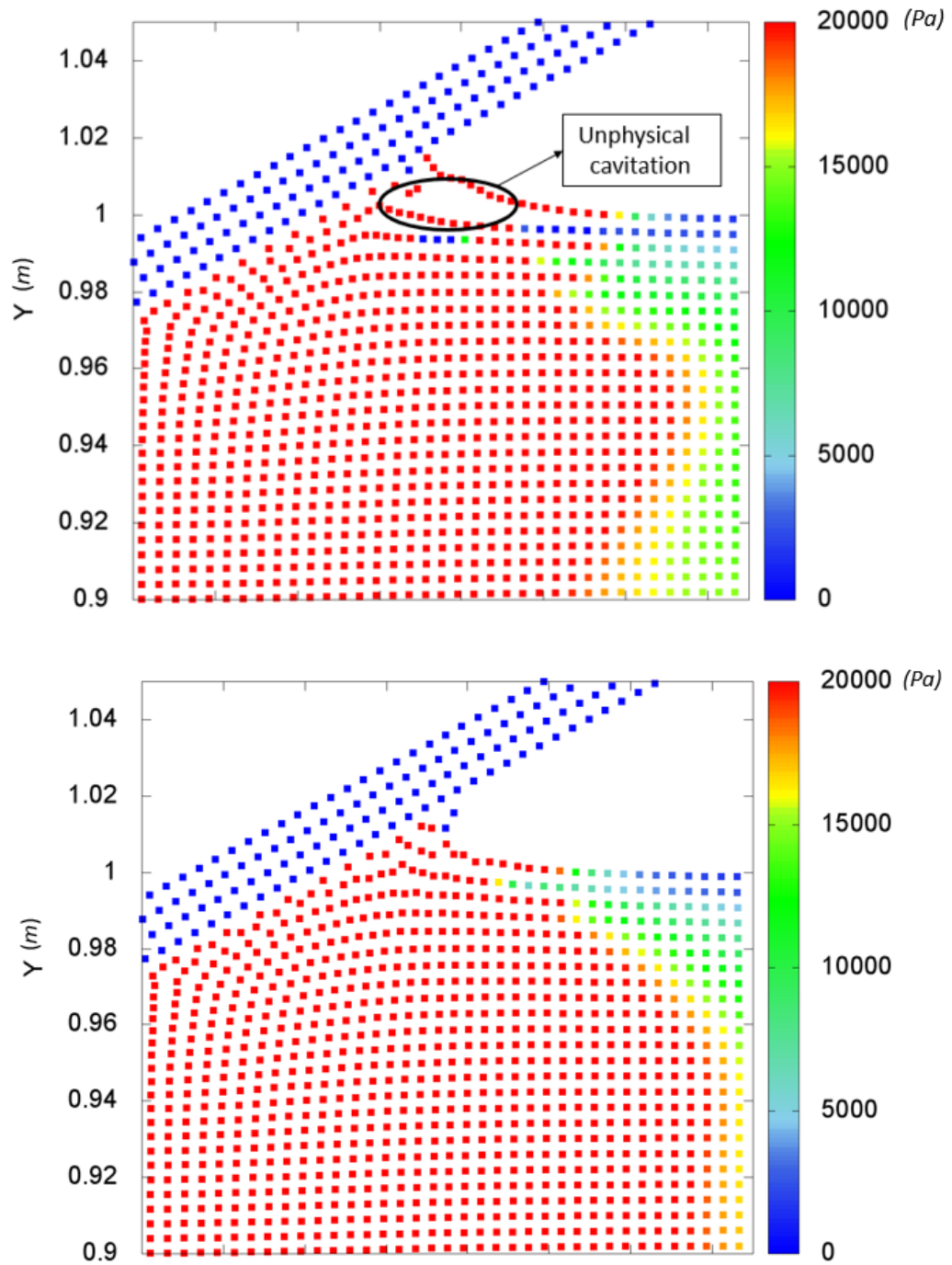


Figure 3.18: Particle distribution profiles predicted by the original SPH method (top) and the present SPH method (below)

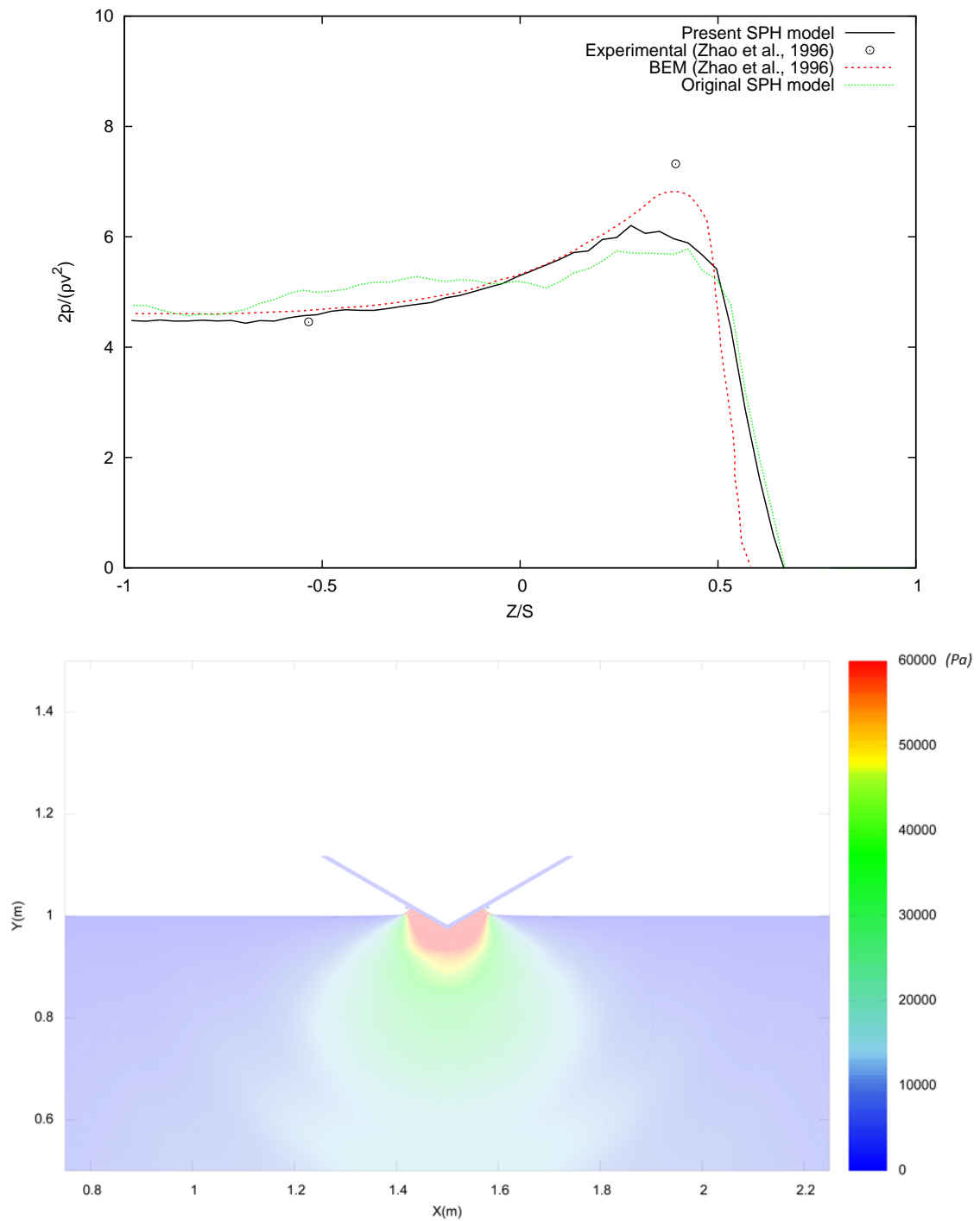


Figure 3.19: Pressure distribution on the wedge at  $t=0.00435s$  and  $ds=B/300$

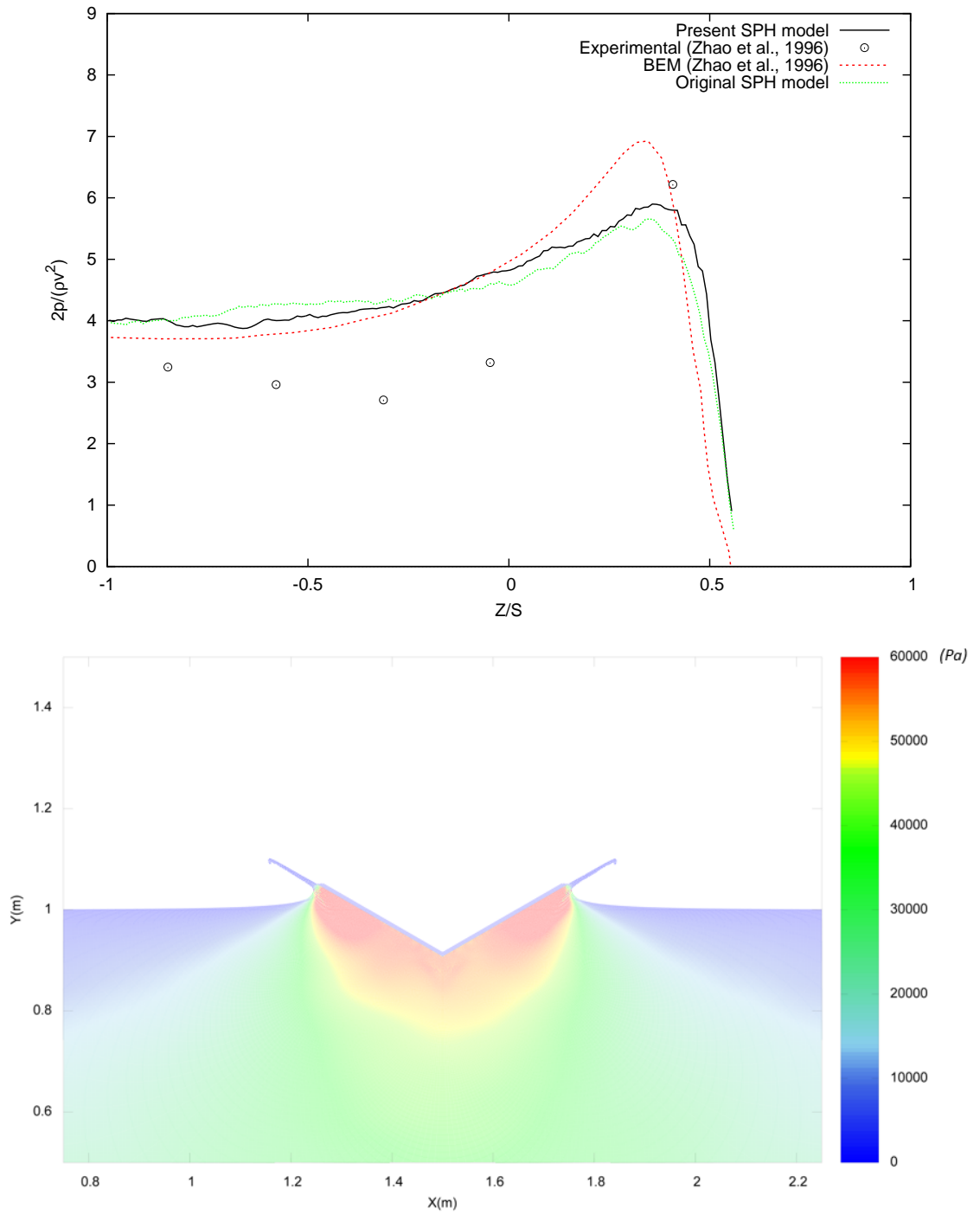


Figure 3.20: Pressure distribution on the wedge  $t=0.0158s$  and  $ds=B/300$

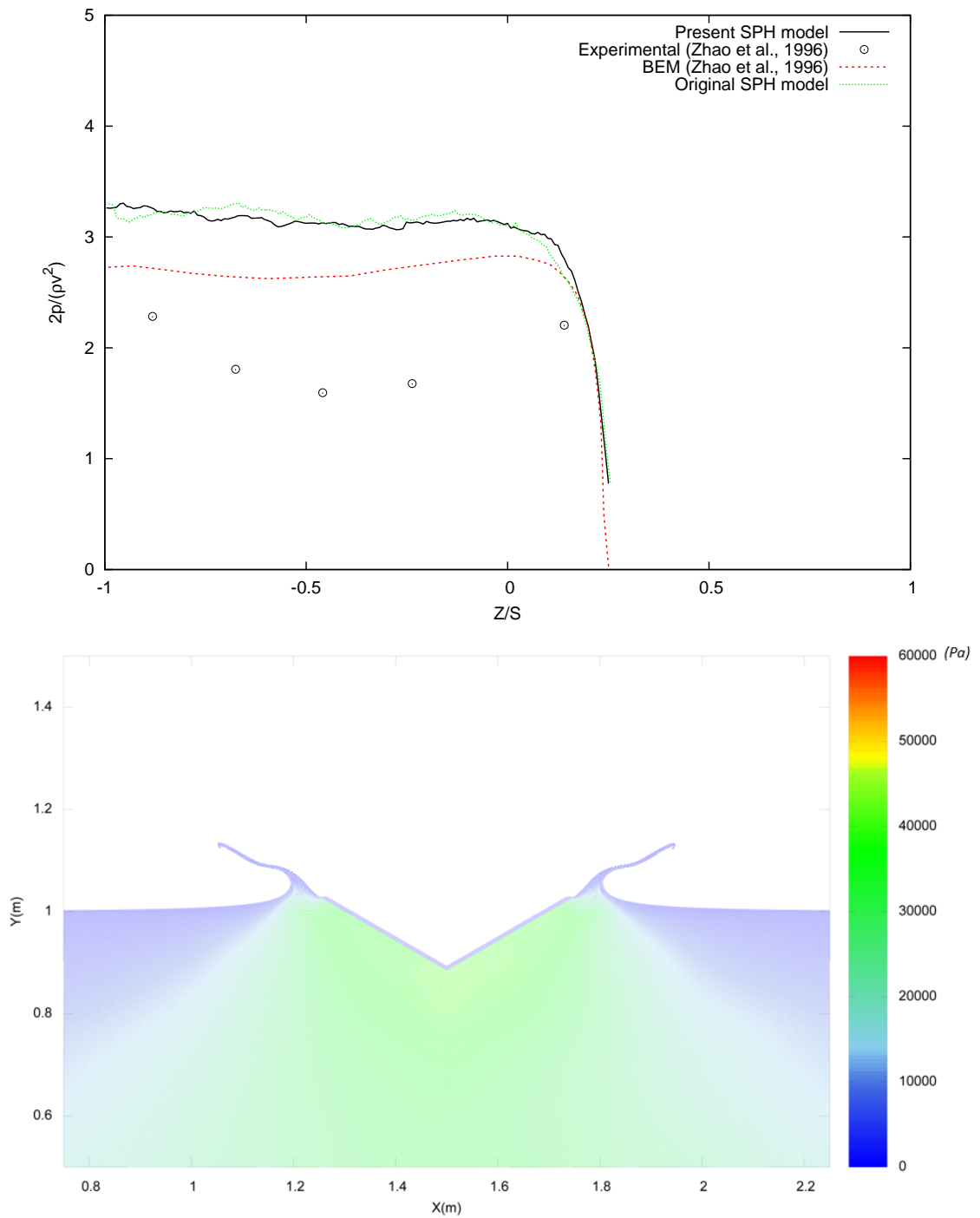


Figure 3.21: Pressure distribution on the wedge at  $t=0.0202s$  and  $ds=B/300$

### 3.3 Sloshing flow

In this section, sloshing flow excited by roll motions was simulated to validate the present SPH algorithm. In the simulations, the tank was modelled with the moving solid boundary, and the impact loads were evaluated and compared with the experimental data.

#### 3.3.1 Case description

The experimental tests were carried out by Delorme et al. (2009). The experimental setup is illustrated in Figure 3.22. The rectangular tank had a length of  $0.900m$ , a height of  $0.508m$  and a width of  $0.310m$ . The filling level of this tank was  $0.093m$ . The pressure sensor was placed on the left wall of the tank ( $0.093m$  above the bottom). The rotation axis was at the center line of the bottom of the tank. At the initial time, the tank was in the horizontal position. The time series of angle and velocity in the experiments are given in Figure 3.23 and Figure 3.24.

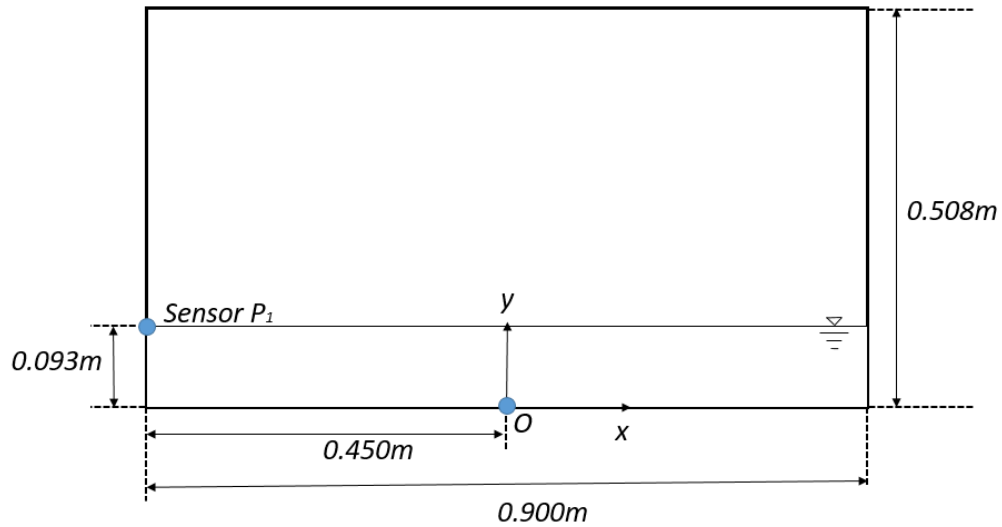


Figure 3.22: Sketch of the setup of the sloshing tank

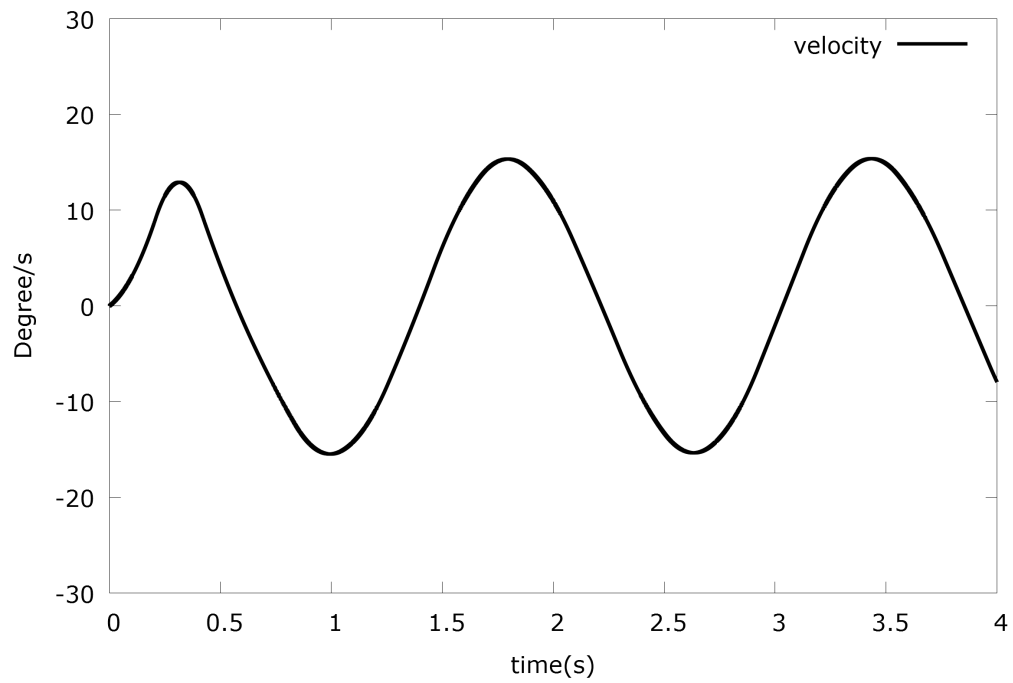


Figure 3.23: Time history of the angular velocity of the tank by Delorme et al. (2009)

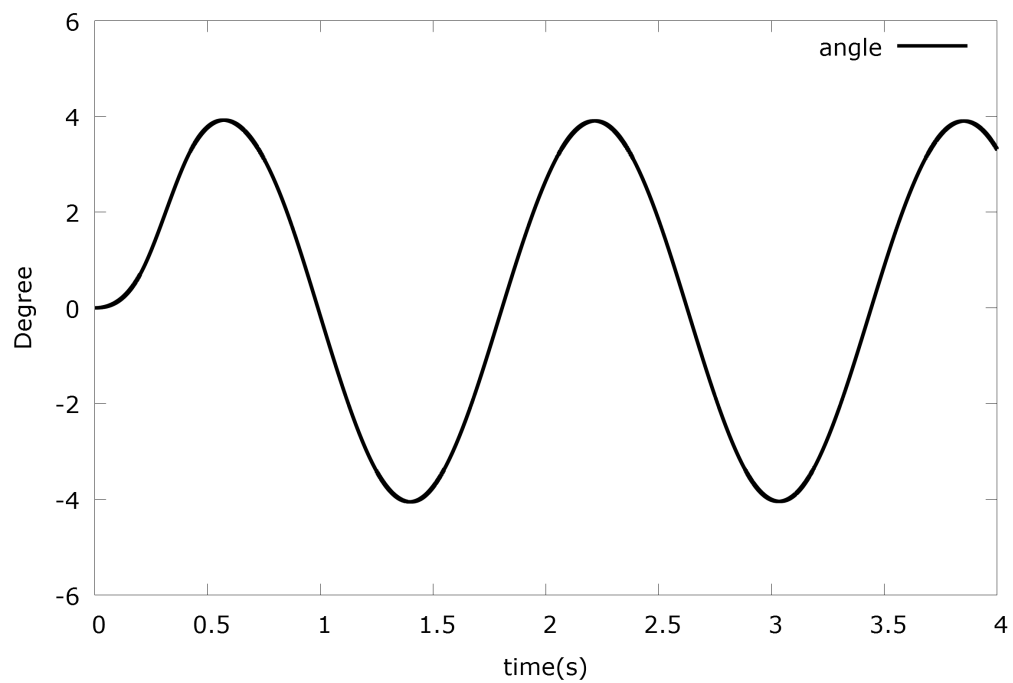


Figure 3.24: Time history of the angle of the tank by Delorme et al. (2009)

### 3.3.2 Convergence study

Convergence studies were carried out for the impact pressure at  $P_1$  using various particle spacing and  $CFL$  numbers. The four particle spacings included  $L/250$ ,  $L/360$ ,  $L/450$  and  $L/500$ , where  $L$  is the length of the tank, corresponding to 6,800, 13,400, 21,150 and 25,900 fluid particles, respectively. In these three cases, a constant  $CFL$  number, 0.2, was used. Another three cases were conducted with different  $CFL$  numbers: 0.20, 0.30, 0.40 and 0.50 with the constant particle spacing of  $L/450$ . As shown in Figure 3.25, the oscillations in the pressure get smaller as the particle spacing decreases. As shown in Figure 3.26, the numerical solutions are not sensitive to the  $CFL$  number.

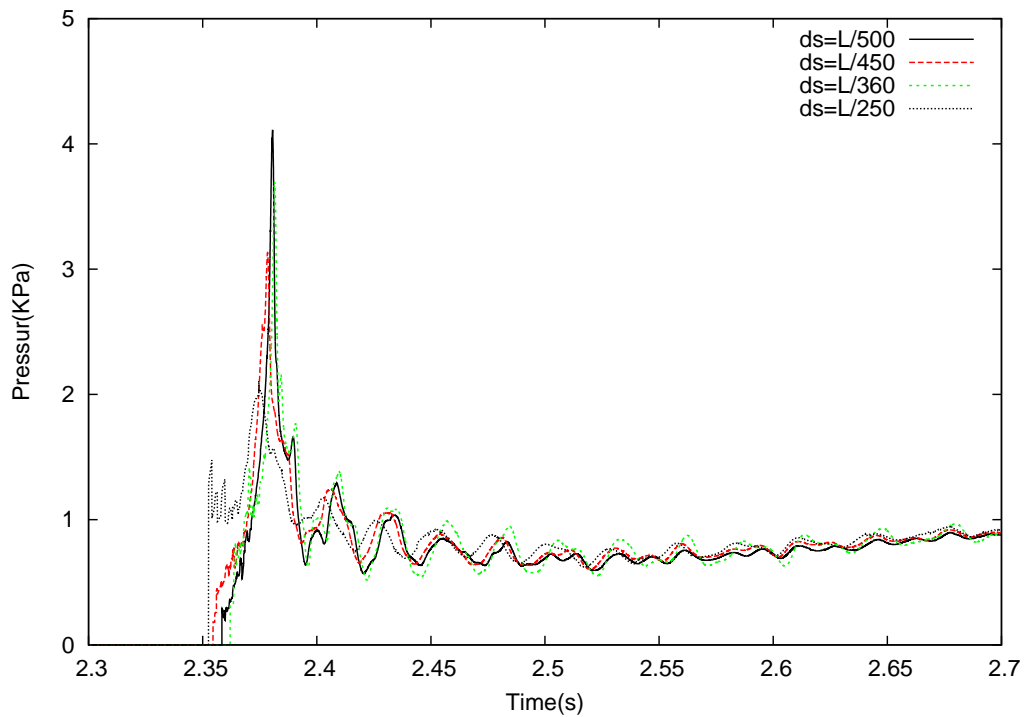


Figure 3.25: Sensitivity of the impact pressure on  $P_1$  to particle spacing

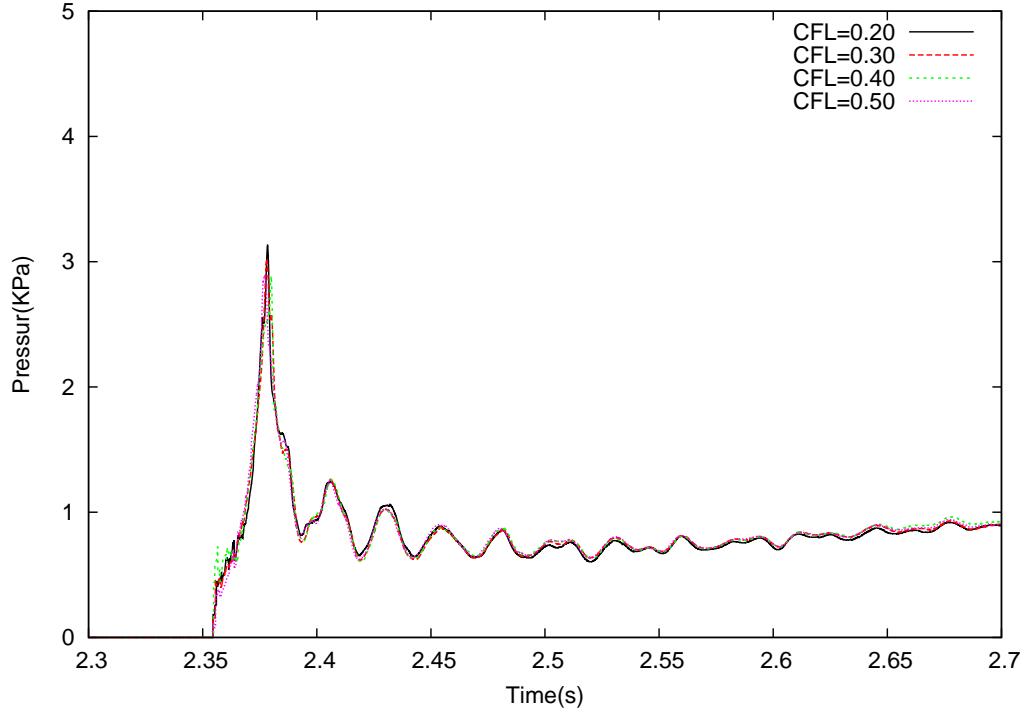


Figure 3.26: Sensitivity of the impact pressure on  $P_1$  to time step size

### 3.3.3 Numerical results

In the following simulations, particle spacing is set to  $L/450$ . 21,150 fluid particles and 4,476 fixed ghost particles were employed to model the water flow and the tank walls, respectively. The  $CFL$  number is set to 0.2. The motions of the tank recorded in the experiments were also used in the simulations. The moving solid boundary conditions were satisfied by using fixed ghost particles, which moved with the tank. The time series of the impact pressure at  $P_1$  are compared with the experimental results in Figure 3.27. The predicted pressure time history is in a reasonable agreement with the experimental one. The maximum pressure is similar to the experimental value. It is also shown that the present method with the particle shift technique gives a closer pressure prediction than the original one. Snapshots of the sloshing flow are also compared with the experimental photo in in Figures 3.28 and 3.29.

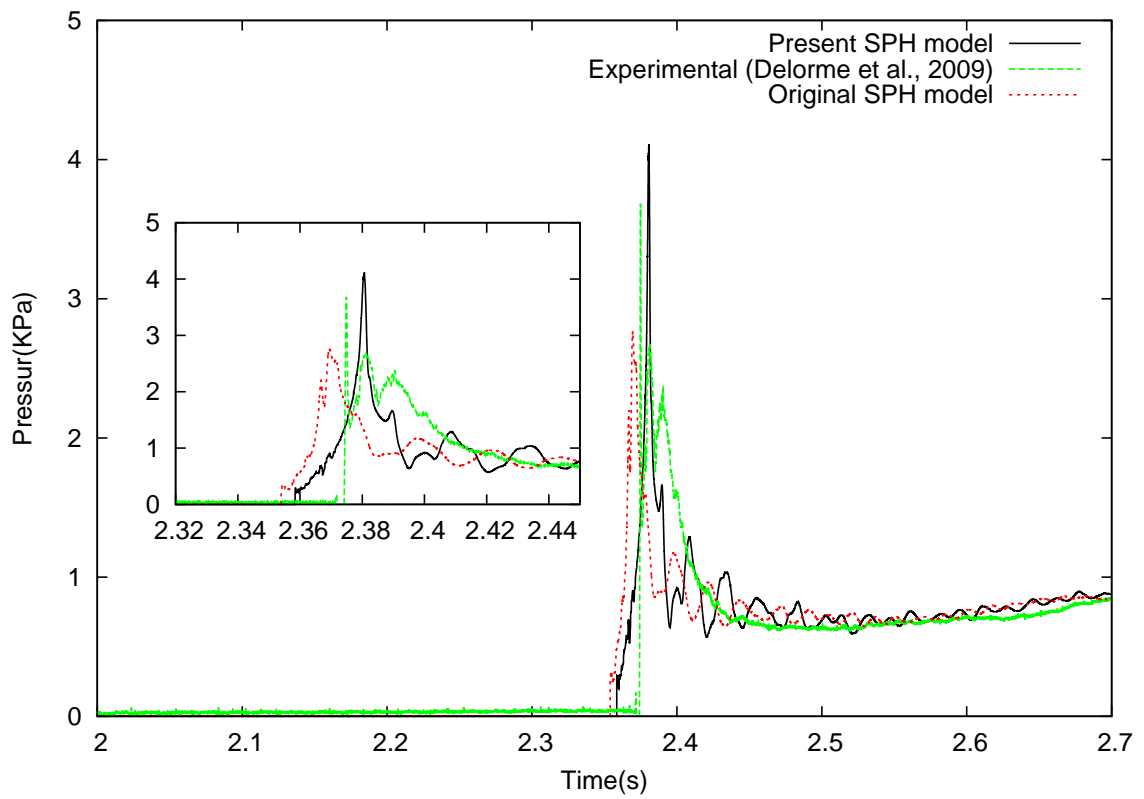


Figure 3.27: Time history of impact pressure on  $P_1$

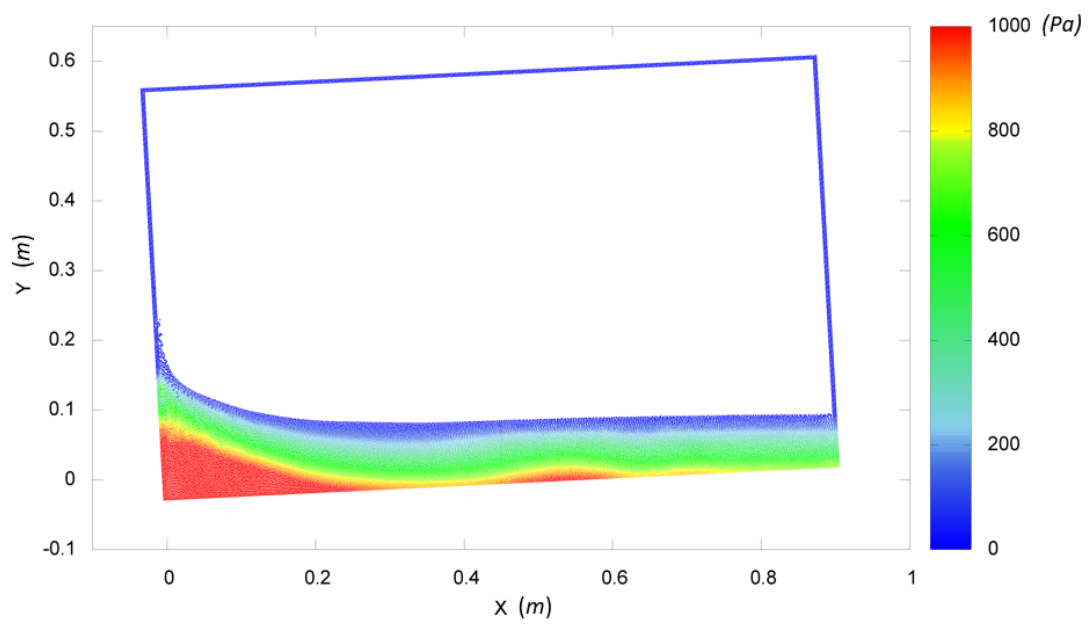
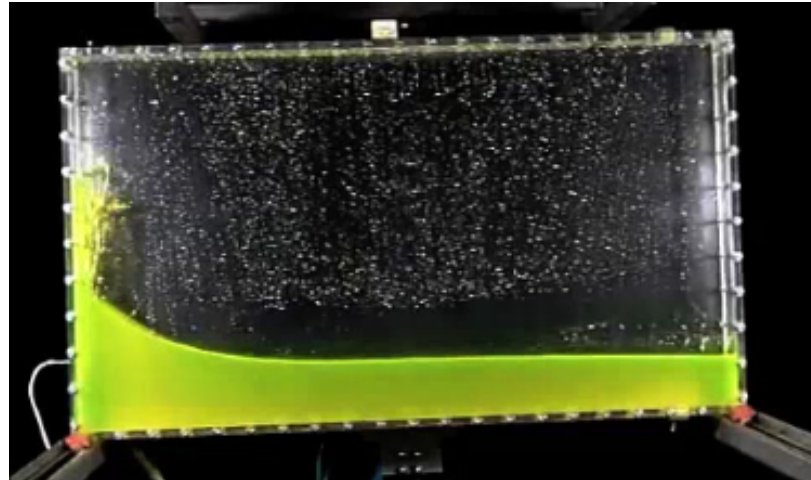


Figure 3.28: Snapshots of the evolution of the sloshing flow at  $t=2.40\text{s}$

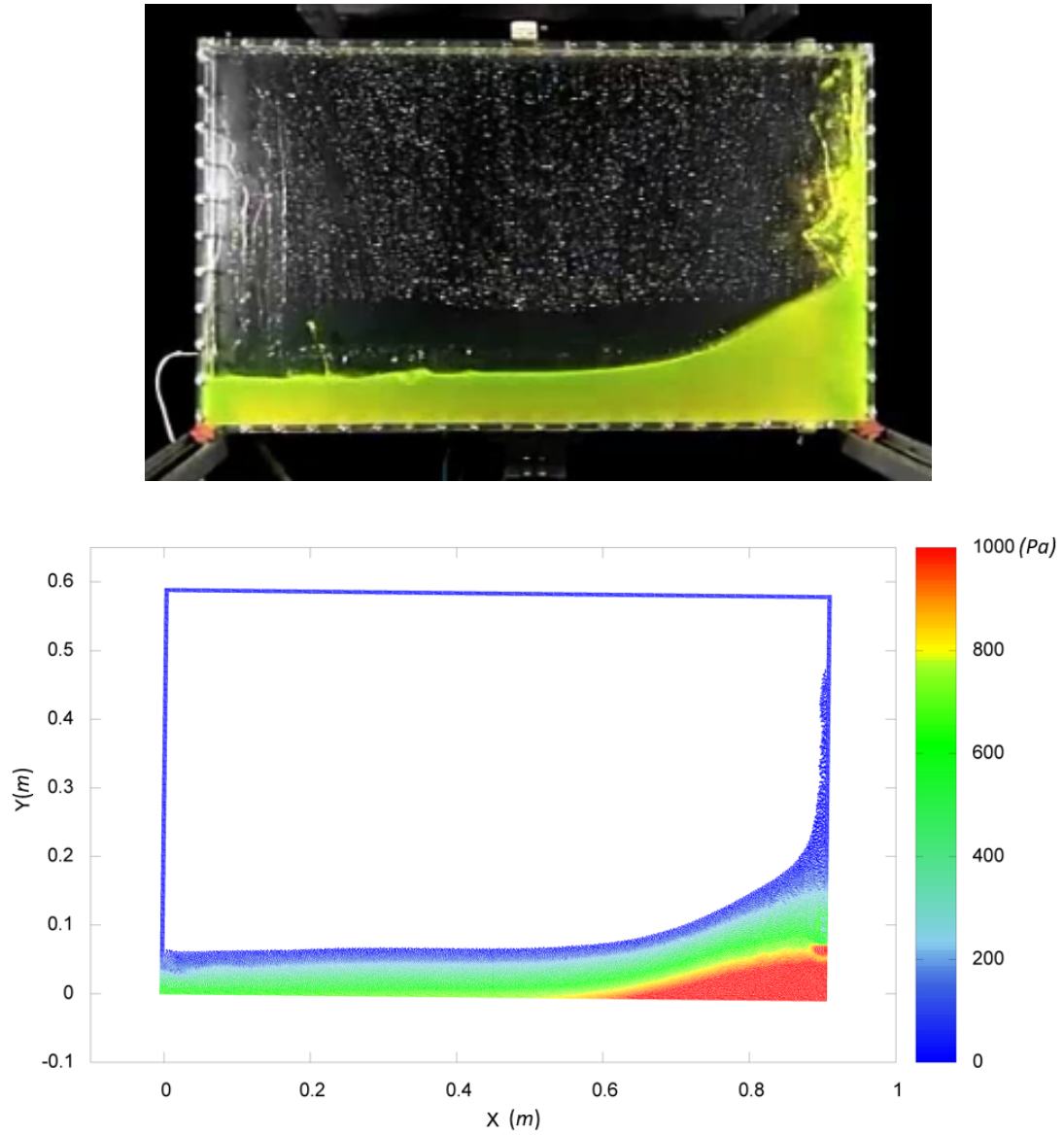


Figure 3.29: Snapshots of the evolution of the sloshing flow at  $t=3.40s$

# Chapter 4

## Conclusions and Future Work

In this thesis, a numerical program based on an improved SPH method was developed to simulate two-dimensional breaking free-surface flow interactions with fixed or moving solid structures by solving the Euler equations. A specified equation of state was employed to link the density field and the pressure field explicitly. An integral interpolation method was used to approximate the physical quantity of the fluid field and its spacial derivatives.

To decrease high-frequency noise in pressure, a numerical viscous term and a diffusive term were added into the equations of momentum and continuity equation, respectively. The solid boundary conditions were modelled with a fixed ghost particle method, which was stable and flexible for various solid boundaries. In this thesis, a particle shift technique was further improved by using background particles, which leads to smoother pressure predictions.

Validation studies were conducted for dam breaking flow against a vertical wall, water entry of a free-fall wedge and sloshing flow in a rectangular tank excited by roll motions. The impact pressure, hydrodynamics forces, and largely deformed free surface were compared with experimental data and good agreement has been achieved.

In conclusion, the present model is robust and accurate in the two-dimensional simulation of the fluid-solid interactions with breaking free surfaces and strong impact in these three cases.

There are still plenty of problems waiting to be addressed. First of all, the present work should be extended to three dimensions for a wider range of applications. When the three-dimensional work is conducted, the computational cost will increase sharply. To make the cost affordable, parallel computation becomes necessary. Another promising approach reducing computational cost is the multi-resolution technique which decreases the number of particles by setting the particles far from the region of interest to larger sizes. When particles with various sizes mix together, problems will appear in the interpolation process. The methods for dealing with neighbour particles of different sizes is still unclear and needs further research.

Another problem is that the present SPH model can only simulate single-phase problems. Air effects such as air entrapment cannot be modelled properly. A reliable two-phase model is necessary to get more accurate solutions for breaking free-surface flows. In the two-phase model, the discontinuity of density near the interfaces makes the interpolation process difficult. New techniques addressing this difficulty are desirable. Considering the numerical instability among air particles can be easily excited, using a meshed-based method to model the air phase is a potential choice. In such case, new interface techniques coupling different CFD methods are necessary. For more extreme breaking free-surface flow, air entrapment plays an important role and has to be considered. Violent flow interaction with structures can cause particle penetration near solid boundary. Appropriate solid boundary method avoiding particle penetration is necessary.

In three-dimensional simulations, enforcing solid boundary conditions becomes complex. The fixed ghost particle method used in the present work faces challenges

handling sharp curvatures. The repellent force method is a straightforward and fast technique to build arbitrary solid boundaries but contribute pressure noise. To apply the SPH method to engineering problems, a robust and accurate solid boundary technique modelling three-dimensional solid boundaries with arbitrary shapes will be advantageous.

# Bibliography

- Antuono, M., Bouscasse, B., Colagrossi, A., and Marrone, S. (2014). A measure of spatial disorder in particle methods. *Computer Physics Communications*, 185(10):2609–2621.
- Antuono, M., Colagrossi, A., Marrone, S., and Lugni, C. (2011). Propagation of gravity waves through an SPH scheme with numerical diffusive terms. *Computer Physics Communications*, 182(4):866–877.
- Antuono, M., Colagrossi, A., Marrone, S., and Molteni, D. (2010). Free-surface flows solved by means of SPH schemes with numerical diffusive terms. *Computer Physics Communications*, 181(3):532–549.
- Bonet, J. and Lok, T. S. (1999). Variational and momentum preservation aspects of smooth particle hydrodynamic formulations. *Computer Methods in Applied Mechanics and Engineering*, 180(1):97–115.
- Bouscasse, B., Colagrossi, A., Marrone, S., and Antuono, M. (2013). Nonlinear water wave interaction with floating bodies in SPH. *Journal of Fluids and Structures*, 42:112–129.
- Chung, T. J. (2010). *Computational fluid dynamics*. Cambridge University Press.
- Colagrossi, A., Antuono, M., and Le Touze, D. (2009). Theoretical considerations

- on the free-surface role in the smoothed-particle-hydrodynamics model. *Physical Review E*, 79(5):056701.
- Colagrossi, A. and Landrini, M. (2003). Numerical simulation of interfacial flows by smoothed particle hydrodynamics. *Journal of Computational Physics*, 191(2):448–475.
- Cummins, S. J. and Rudman, M. (1999). An SPH projection method. *Journal of Computational Physics*, 152(2):584–607.
- Dalrymple, R. A., Knio, O., Cox, D. T., Gesteira, M., and Zou, S. (2002). Using a lagrangian particle method for deck overtopping. In *Ocean Wave Measurement and Analysis (2001)*, pages 1082–1091.
- Delorme, L., Colagrossi, A., Souto-Iglesias, A., Zamora-Rodriguez, R., and Botia-Vera, E. (2009). A set of canonical problems in sloshing, part i: Pressure field in forced roll—comparison between experimental results and SPH. *Ocean Engineering*, 36(2):168–178.
- Ellero, M., Serrano, M., and Espanol, P. (2007). Incompressible smoothed particle hydrodynamics. *Journal of Computational Physics*, 226(2):1731–1752.
- Fries, T. and Matthies, H. (2003). Classification and overview of meshfree methods. *Technical University Braunschweig*.
- Gingold, R. A. and Monaghan, J. J. (1977). Smoothed particle hydrodynamics: theory and application to non-spherical stars. *Monthly Notices of the Royal Astronomical Society*, 181(3):375–389.
- Gingold, R. A. and Monaghan, J. J. (1982). Kernel estimates as a basis for general

- particle methods in hydrodynamics. *Journal of Computational Physics*, 46(3):429–453.
- Gomez-Gesteira, M., Cerqueiro, D., Crespo, C., and Dalrymple, R. A. (2005). Green water overtopping analyzed with a SPH model. *Ocean Engineering*, 32(2):223–238.
- Gotoh, H., Khayyer, A., Ikari, H., Arikawa, T., and Shimosako, K. (2014). On enhancement of incompressible SPH method for simulation of violent sloshing flows. *Applied Ocean Research*, 46:104–115.
- Haque, A. and Dilts, G. A. (2007). Three-dimensional boundary detection for particle methods. *Journal of Computational Physics*, 226(2):1710–1730.
- Khayyer, A. and Gotoh, H. (2009). Wave impact pressure calculations by improved SPH methods. *International Journal of Offshore and Polar Engineering*, 19(04).
- Khayyer, A., Gotoh, H., and Shimizu, Y. (2017). Comparative study on accuracy and conservation properties of two particle regularization schemes and proposal of an optimized particle shifting scheme in isph context. *Journal of Computational Physics*, 332:236–256.
- Landrini, M., Colagrossi, A., and Faltinsen, O. M. (2003). Sloshing in 2-d flows by the SPH method. In *8th International Conference on Numerical Ship Hydrodynamics, Busan, Korea*, pages 22–25.
- Landrini, M., Colagrossi, A., Greco, M., and Tulin, M. P. (2007). Gridless simulations of splashing processes and near-shore bore propagation. *Journal of Fluid Mechanics*, 591:183–213.
- Le Touze, D., Marsh, A., Oger, G., Guilcher, P., Khaddaj, M. C., Alessandrini, B.,

- and Ferrant, P. (2010). SPH simulation of green water and ship flooding scenarios. *Journal of Hydrodynamics, Ser. B*, 22(5):231–236.
- Lind, S. J., Xu, R., Stansby, P. K., and Rogers, B. D. (2012). Incompressible smoothed particle hydrodynamics for free-surface flows: A generalised diffusion-based algorithm for stability and validations for impulsive flows and propagating waves. *Journal of Computational Physics*, 231(4):1499–1523.
- Lobovsky, L., Botia-Vera, E., Castellana, F., Mas-Soler, J., and Souto-Iglesias, A. (2014). Experimental investigation of dynamic pressure loads during dam break. *Journal of Fluids and Structures*, 48:407–434.
- Lucy, L. B. (1977). A numerical approach to the testing of the fission hypothesis. *The Astronomical Journal*, 82:1013–1024.
- Marrone, S. (2012). *Enhanced SPH modeling of free-surface flows with large deformations*. PhD thesis, Sapienza University of Rome.
- Marrone, S., Antuono, M., Colagrossi, A., Colicchio, G., Le Touze, D., and Graziani, G. (2011).  $\delta$ -SPH model for simulating violent impact flows. *Computer Methods in Applied Mechanics and Engineering*, 200(13):1526–1542.
- Marrone, S., Colagrossi, A., Le Touze, D., and Graziani, G. (2010). Fast free-surface detection and level-set function definition in SPH solvers. *Journal of Computational Physics*, 229(10):3652–3663.
- Maruzewski, P., Le Touze, D., Oger, G., and Avellan, F. (2010). SPH high-performance computing simulations of rigid solids impacting the free-surface of water. *Journal of Hydraulic Research*, 48(S1):126–134.

- Mei, C. C. (1989). *The Applied Dynamics of Ocean Surface Waves*, volume 1. World Scientific.
- Molteni, D. and Colagrossi, A. (2009). A simple procedure to improve the pressure evaluation in hydrodynamic context using the SPH. *Computer Physics Communications*, 180(6):861–872.
- Monaghan, J. J. (1994). Simulating free surface flows with SPH. *Journal of Computational Physics*, 110(2):399–406.
- Monaghan, J. J. (2000). SPH without a tensile instability. *Journal of Computational Physics*, 159(2):290–311.
- Monaghan, J. J. (2005). Smoothed particle hydrodynamics. *Reports on Progress in Physics*, 68(8):1703.
- Monaghan, J. J. and Gingold, R. A. (1983). Shock simulation by the particle method SPH. *Journal of Computational Physics*, 52(2):374–389.
- Monaghan, J. J. and Kajtar, J. B. (2009). SPH particle boundary forces for arbitrary boundaries. *Computer Physics Communications*, 180(10):1811–1820.
- Monaghan, J. J. and Kos, A. (1999). Solitary waves on a cretan beach. *Journal of waterway, port, coastal, and ocean engineering*, 125(3):145–155.
- Monaghan, J. J. and Kos, A. (2000). Scott russell’s wave generator. *Physics of Fluids*, 12(3):622–630.
- Morris, J. P. (1996). A study of the stability properties of smooth particle hydrodynamics. *Publications of the Astronomical Society of Australia*, 13:97–102.
- Naito, S. and Sueyoshi, M. (2002). A numerical study on complicated motions of floating bodies. In *Sixth International Ship Stability Workshop, New York*.

- Oger, G., Alessandrini, B., and Ferrant, P. (2005). Capture of air cushion effects in a wedge water entry SPH simulation. In *The Fifteenth International Offshore and Polar Engineering Conference*. International Society of Offshore and Polar Engineers.
- Oger, G., Doring, M., Alessandrini, B., and Ferrant, P. (2006). Two-dimensional SPH simulations of wedge water entries. *Journal of Computational Physics*, 213(2):803–822.
- Oger, G., Doring, M., Leroyer, A., Alessandrini, B., and Visonneau, M. (2004). SPH and finite volume simulations of a wedge water entry. In *The Fourteenth International Offshore and Polar Engineering Conference*. International Society of Offshore and Polar Engineers.
- Omidvar, P., Stansby, P. K., and Rogers, B. D. (2012). Wave body interaction in 2D using smoothed particle hydrodynamics (SPH) with variable particle mass. *International Journal for Numerical Methods in Fluids*, 68(6):686–705.
- Omidvar, P., Stansby, P. K., and Rogers, B. D. (2013). SPH for 3D floating bodies using variable mass particle distribution. *International Journal for Numerical Methods in Fluids*, 72(4):427–452.
- Rafiee, A., Cummins, S., Rudman, M., and Thiagarajan, K. (2012). Comparative study on the accuracy and stability of SPH schemes in simulating energetic free-surface flows. *European Journal of Mechanics-B*, 36:1–16.
- Rafiee, A., Elsaesser, B., and Dias, F. (2013). Numerical simulation of wave interaction with an oscillating wave surge converter. In *32nd International Conference on Ocean, Offshore and Arctic Engineering*. American Society of Mechanical Engineers.

- Servan-Camas, B., Cercos-Pita, J. L., Colom-Cobb, J., Garcia-Espinosa, J., and Souto-Iglesias, A. (2016). Time domain simulation of coupled sloshing–seakeeping problems by SPH-FEM coupling. *Ocean Engineering*, 123:383–396.
- Shao, S. D. (2009). Incompressible SPH simulation of water entry of a free-falling object. *International Journal for Numerical Methods in Fluids*, 59(1):91–115.
- Shao, S. D. and Lo-Edmond, Y. M. (2003). Incompressible SPH method for simulating newtonian and non-newtonian flows with a free surface. *Advances in Water Resources*, 26(7):787–800.
- Shibata, K., Koshizuka, S., Sakai, M., and Tanizawa, K. (2012). Lagrangian simulations of ship-wave interactions in rough seas. *Ocean Engineering*, 42:13–25.
- Souto-Iglesias, A., Delorme, L., Perez-Rojas, L., and Abril-Perez, S. (2006). Liquid moment amplitude assessment in sloshing type problems with smooth particle hydrodynamics. *Ocean Engineering*, 33(11):1462–1484.
- Souto-Iglesias, A., Perez-Rojas, L., and Zamora-Rodríguez, R. (2003). Simulation of anti-roll tanks and sloshing type problems with smoothed particle hydrodynamics. *Ocean Engineering*, 31(8):1169–1192.
- Sun, P. N., Colagrossi, A., Marrone, S., and Zhang, A. M. (2017). The  $\delta$ plus-SPH model: Simple procedures for a further improvement of the SPH scheme. *Computer Methods in Applied Mechanics and Engineering*, 315:25–49.
- Takeda, H., Miyama, S. M., and Sekiya, M. (1994). Numerical simulation of viscous flow by smoothed particle hydrodynamics. *Progress of Theoretical Physics*, 92(5):939–960.

- Tezduyar, T. (2002). Interface-tracking and interface-capturing techniques for computation of moving boundaries and interfaces. In *Proceedings of the Fifth World Congress on Computational Mechanics*.
- Ulrich, C. and Rung, T. (2012). Multi-physics SPH simulations of launching problems and floating body interactions. In *31st International Conference on Ocean, Offshore and Arctic Engineering*, pages 685–694. American Society of Mechanical Engineers.
- Veen, D. J. and Gourlay, T. P. (2011). A 2D smoothed particle hydrodynamics theory for calculating slamming loads on ship hull sections. In *High Speed Marine Vessels Conference, Fremantle, Australia*.
- Veen, D. J. and Gourlay, T. P. (2012). A combined strip theory and smoothed particle hydrodynamics approach for estimating slamming loads on a ship in head seas. *Ocean Engineering*, 43:64–71.
- Xu, R., Stansby, P., and Laurence, D. (2009). Accuracy and stability in incompressible SPH (ISPH) based on the projection method and a new approach. *Journal of Computational Physics*, 228(18):6703–6725.
- Zhao, R., Faltinsen, O., and Aarsnes, J. (1996). Water entry of arbitrary two-dimensional sections with and without flow separation. In *Proceedings of the 21st Symposium on Naval Hydrodynamics*, pages 408–423.